Evaluating BC and NOx emission inventories for the Paris region from MEGAPOLI aircraft measurements

H. Petetin[1], M. Beekmann[1], A. Colomb[1,3], H. A. C. Denier van der Gon[4], J.-C. Dupont[5], C. Honoré[6], V. Michoud[1,7], Y. Morille[5], O. Perrussel[6], A. Schwarzenboeck[3], J. Sciare[8], A. Wiedensohler[9], Q. J. Zhang[1,2]

(1) {LISA/IPSL, Laboratoire Interuniversitaire des Systèmes Atmosphériques, UMR CNRS 7583, Université Paris Est Créteil (UPEC) et Université Paris Diderot (UPD), France.}

(2) {now at : ARIA, Boulogne-Billancourt, France}

(3) {Laboratoire de Météorologie Physique, Clermont-Ferrand, France}

(4) {TNO, Princetonlaan 6, 3584 CB Utrecht, The Netherlands}

(5) {Laboratoire de Météorologie Dynamique, Palaiseau, France}

(6) {AIRPARIF, Agence de surveillance de la qualité de l'air, Paris, France}

(7) {now at: Mines Douai, SAGE, Douai, France}

(8) {LSCE, Laboratoire des Sciences du Climat et de l'Environnement, CNRS-CEA-UVSQ, Gif-sur-Yvette, France}

(9) {Leibniz-Institute for Tropospheric Research, Leipzig, Germany}

Correspondence to: H. Petetin (herve.petetin@lisa.u-pec.fr)

Abstract

High uncertainties affect black carbon (BC) emissions and, despite its important impact on air pollution and climate, very few BC emissions evaluations are found in the literature. This paper presents a novel approach, based on airborne measurements across the Paris, France, plume, developed in order to evaluate BC and NO_x emissions at the scale of a whole agglomeration. The methodology consists in integrating, for each transect, across the plume observed and simulated concentrations above background. This allows minimizing several error sources in the used model (e.g. representativeness, chemistry, plume lateral dispersion). The procedure is applied with the CHIMERE chemistry-transport model to three inventories — the EMEP inventory, and the so-called TNO and TNO-MP inventories — over the month of July 2009. Various systematic uncertainty sources both in the model (e.g. boundary layer height, vertical mixing, deposition) and in observations (e.g. BC nature) are discussed and quantified, notably through sensitivity tests. Large uncertainty values are determined in our results, which limits the usefulness of the method to rather strongly erroneous emission inventories. A statistically significant (but moderate) overestimation is

1 obtained on the TNO BC emissions and on EMEP and TNO-MP NO_x emissions, as well as on the

2 BC/NOx emission ratio in TNO-MP. The benefit of the airborne approach is discussed through a

3 comparison with the BC/NO_x ratio at a ground site in Paris, which additionally suggests a spatially

4 heterogeneous error in BC emissions over the agglomeration.

5 **1   Introduction**

6 Knowledge on pollutant emissions is a key element in the field of air pollution. It provides essential

7 information on the contribution of various source sectors to pollutant levels, which is required for

8 targeting emission reduction measures. Emission inventories are necessary input to chemistry-

9 transport models (CTMs) which are important tools for atmospheric research and air quality

10 management.

11 Among the various emitted species, black carbon (BC) aerosol is a chemical compound of major

12 importance. In air quality, it highly contributes to the health risk (Peng et al., 2009) related to fine

13 particulate matter ($PM_{2.5}$, particulate matter with aerodynamic diameter below 2.5 μm). It also plays a

14 crucial role in the Earth's climate through the scattering and the absorption of incoming solar

15 radiation and the subsequent change in planetary albedo (direct effect) (Schulz et al., 2006; Yu et al.,

16 2006) and the modification of cloud properties as BC when coated with hydrophilic species acts as

17 cloud condensation nuclei (indirect effect) (Lohmann and Feichter, 2005). The overall industrial era

18 BC radiative forcing (including direct, semi-direct and indirect effects, as well as albedo change due

19 to deposition on snow) is estimated at +1.1 W m^{-2}, ranking second between the carbon dioxide

20 (CO_2, +1.56 W m^{-2}) and methane (CH_4, +0.86 W m^{-2}) forcing (Bond et al., 2013).

21 However, high uncertainties still affect BC emission inventories making the true forcing uncertain.

22 As a product of incomplete combustion processes, BC emissions at the global scale mainly originate

23 from energy-related combustion (e.g. on- and off-road vehicles in transport area, biofuel and coal in

24 residential area) and open burning (savannas and forest fires) (Bond et al., 2004, 2013; Junker and

25 Liousse, 2008; Lamarque et al., 2010). Global BC emissions are most recently estimated at 7.5 Tg

26 year^{-1}, with an uncertainty range of 2-29 Tg year^{-1}, of which 4.8 Tg

27 year^{-1} originate from energy-related combustion (1.2-15 Tg year^{-1}) (Bond et al., 2013). Most values

28 given in the literature are included in this large (factor 10) range. Granier et al. (2011) compared

29 inventories over the past decades at different scales. In 2005, the ratio of the highest over the lowest

30 global BC emissions estimate is only 1.28, but higher values are given at the regional scale in

31 Western and Central Europe, with ratios of 1.34 and 1.76, respectively. Uncertainties arise from

32 emission factors (usually highly dependent on the conditions of use and the type of equipment),

33 activity data and spatial distribution for some source sectors (e.g. wood burning heating). By

34 analysing a large number of source profiles, Chow et al. (2011) found highly variable BC contents in

35 different $PM_{2.5}$ emission factors, in the range of 6-37% for on-road light-duty gasoline engine

1   exhausts, 33-74% for on-road heavy-duty diesel engine exhausts, 29-61% for tire wear, 6-13% for

2   agricultural burning, 4-33% for residential wood combustion and 3-14% for oil combustion

3   stationary sources. Dallmann and Harley (2010) have quantified uncertainties in $PM_{2.5}$ emission

4   factors for various mobile sources, such as on-road gasoline (±45%) and on-road diesel (±59%)

5   sources. On the contrary, the authors have estimated a much lower uncertainty in fuel consumption,

6   around ±3 and ±5% for on-road gasoline and diesel vehicles, respectively. In the evaluation of the BC

7   climate impact, these uncertainties on emissions contribute — among other uncertainty sources such

8   as microphysical interactions in clouds or removal processes — to a large 95% confidence interval on

9   the BC radiative forcing, between +0.17 and +2.1 W m^{-2} (Bond et al., 2013). It is worthwhile noting

10   that deducing local/regional scale BC emission uncertainties (for instance over the Paris megacity)

11   from those at global scale, appears tricky. Indeed, if on the one hand uncertainties usually increase

12   when considering smaller domains (because of uncertainties in spatial distribution of emissions), on

13   the other hand some uncertainty sources relevant at global scale may be reduced at European scale

14   (e.g. minor contribution of highly uncertain open burning emissions, better constrained local activity

15   data). This is notably the case of a megacity like Paris located in a post-industrial country where the

16   most uncertain sources have a low contribution.

17   Compared to BC, much more efforts have been made to assess NO_x emissions that in turn appear

18   better constrained. In the inventories inter-comparison of Granier et al. (2011), the ratios between the

19   highest and lowest NO_x emissions are 1.15 at global scale, and 1.18 and 1.23 in Western and Central

20   Europe, respectively. Due to real-time measurements, large point sources emissions are expected to

21   be reasonably estimated in countries with mandatory emission monitoring. Concerning the traffic

22   source, which dominates the overall emissions (particularly in summer), uncertainties are still

23   substantial. In bottom-up inventories, these emissions are usually estimated with traffic emission

24   models of various types and complexities. Most uncertainties arise from both activity data and

25   emission factors. Activity data are difficult to estimate as the fleet and its technological

26   characteristics (e.g. Euro standards) are perpetually evolving. Concerning emission factors, various

27   techniques are available, both under controlled conditions or in real-world, and difficulties come up

28   with their combination (see Franco et al., 2013 for a review). Compared to uncertainties previously

29   given for $PM_{2.5}$ emission factors from Dallmann and Harley (2010), uncertainties for NO_x emission

30   factors are significantly lower, with values around ±27 and ±22% for on-road gasoline and on-road

31   diesel sources, respectively. Smit et al. (2010) have reviewed results from 50 studies dealing with the

32   validation of traffic emission models, and have pointed out a tendency to overestimate NO_x emissions

33   whatever the validation techniques (e.g. tunnel, on-board or ambient concentration studies) or the

34   model type (e.g. average-speed, traffic situation or modal model) employed. In their critical

35   evaluation of on-road vehicle emission inventories over the United States, Parrish (2006) indicated

36   rather accurate NO_x inventories in the 1990's but decreasing NO_x emission estimates during the last

decade in contradiction with the tendency inferred from the evolution of NO_x concentrations. Additionally, in Monte-Carlo analysis where uncertainties on NO_x emissions are often considered, the two-sigma uncertainty ranges fixed for traffic NO_x emissions, usually taken from the literature and/or expert judgments, vary substantially in the literature : ±80% (whatever the source) in Deguillaume et al. (2007) (deduced from the ±40% one-sigma uncertainty given in the paper), ±100% for area sources (and ±50% for point sources) in Hanna et al. (2001) (also used in Tian et al. (2010)), ±50% for area sources (and ±3% for point sources) in Napelenok et al. (2011).

The evaluation of these inventories still remains a critical point since emissions are generally not directly measurable. The use of CTMs for direct comparisons between measured and simulated concentrations is most of time inadequate to draw precise conclusions on emission inventories because concentrations measured at a receptor point cannot be unambiguously linked to emissions at a point aloft because of mixing processes and chemical transformations. In addition, CTMs and the meteorological input data they are using have their own uncertainties. Different alternative approaches have thus been developed. Concerning the BC emissions, useful information may be gained from their evaluation relatively to those of another compound for which uncertainty in emissions is expected to be smaller. For example Zhou et al. (2009) derived BC emissions in two Chinese megacities from CO emissions and measured BC/CO ratios at sites 10-15 km downwind of the cities. However, given the large size of these megacities, the measurement representativeness for the city emissions remains an open question. Other methods specifically assess transport patterns of emissions to the receptor point. Xu et al. (2013) have developed a method based on in-situ measurements and backward trajectory analyses to evaluate BC emissions over the North China Plain. A promising approach consists in using inverse modeling techniques, which were widely applied to NO_x emissions using variationnal data assimilation (Mendoza-Dominguez and Russell, 2000), Bayesian Monte-Carlo approaches (Deguillaume et al., 2007, Konovalov et al., 2008), Kalman Filter approaches (Napelenok et al., 2008; Gilliland and Abbitt, 2001). NO_2 columns retrieved by satellites (e.g. form GOME, SCIAMACHY, OMI, GOME-2) provide a valuable observational basis for many of these works because of their large data coverage. For BC, the only study using variationnal data assimilation we are aware of is the one of Hakami et al. (2005) that aims at better constraining BC emissions over East Asia from in-situ measurements.

The aim of this paper is to evaluate emission inventories at the scale of a large city. In this frame, it presents an original methodology based on airborne measurements in the city plume and chemistry-transport simulations. It is applied to BC and NO_x emission inventories over the Paris megacity, with the CHIMERE model. Observations used in this study were obtained in an intensive campaign that took place in and around the city in July 2009 in the framework of the MEGAPOLI European project (Megacity : emission, urban, regional and global atmospheric pollution and climate effect, and

integrated tools for assessment and mitigation; www.megapoli.info). In particular, our study relies on airborne BC measurements in the city plume, trying thus to alleviate problems of representativeness of ground based in-situ measurements. In Sect. 2, the general methodology is described. All input data, including measurement data, emission inventories, and the CHIMERE model, are described in Sect. 3. Results from both ground and airborne measurements are discussed and compared in Sect. 4.

2 Methodology

The method developed in this study aims at evaluating, at the scale of a large city, emission inventories of species that can be traced at the scale of a few hours, i.e. either a chemically inert (at the time scale considered) single compound or a conservative family of products all originating from a unique primary compound. The method is based on airborne measurements of such species in the megacity plume during the afternoon in a well-mixed convective boundary layer (BL), so that the vertical mixing can be considered as rather well established, and consequently the measured concentrations at a particular altitude as representative of concentrations in the whole BL.

A CTM simulation, using the inventory to be evaluated, is used to simulate tracer concentrations in the plume. For both observations and simulations, along the flight path perpendicular to the plume, tracer concentrations above regional background and within the pollution plume can be integrated. The ratio of the simulated area over the measured area corresponds to a spatially averaged emission error factor (EEF) for the agglomeration for each flight. To achieve such a calculation, the plume needs to be well distinguishable from background, which requires large enough local emissions in the city and a rather homogeneous background.

This method aims at reducing the influence of some errors in the CTM. By considering integrated peak areas over lateral transects across the plume, it allows minimizing the effect of some potential errors in the structure of the simulated plume, e.g. any error on lateral dispersion, reasonable errors in wind direction, and consequently to focus more on emissions. However, several potential error sources still remain, and therefore need to be carefully investigated : (i) the wind speed which directly determines the temporal window of emissions sampled during the flight, (ii) the degree of vertical mixing which determines the representativeness of the airborne measured concentrations, (iii) the wet and dry deposition of the tracer which can lead to discrepancies in the emissions factors if not well simulated by the model, and (iv) the boundary layer height that directly affects the level of concentrations. These points will all be discussed in the next sections.

The methodology is applied in this paper to BC and NO_x emissions. As a chemically inert compound, BC can be directly used as a tracer. For the NO_x compounds, as they undergo many fast chemical reactions, the NO_y family gathering all reactive nitrogen species (e.g. NO_x, NO_3, HNO_3, $HONO$, N_2O_5, PAN…) appears more conservative at the time scale of a plume, and is thus used as a tracer of NO_x emissions.

3 Input data

3.1 Measurement data base

In the framework of the EU FP7 MEGAPOLI project (Baklanov et al., 2010), two one-month intensive campaigns (July 2009 and January/February 2010) have been organized in the Greater Paris area to better characterize organic aerosol in a large megacity. The study presented here is based on observations obtained during the summer campaign.

Petzold et al. (2013) have recently made some recommendations about the use of the term "BC" for black carbon, distinguishing various terminologies depending on the property used in the measurement technique: (i) the light absorbing coefficient σ_{ap}, or equivalent BC (EBC) if the MAC is indicated, for instruments based on light absorption, (ii) refractory BC (rBC) for instruments based on refractory properties, (iii) elemental carbon (EC) for instruments focusing on the chemical composition or the carbon content based on thermo-optical methods. So far in this paper, the term BC has been employed as a qualitative and commonly used terminology. In this section, the terminology of Petzold et al. (2013) is used.

Ground measurements of light absorption coefficient, EC and NO_x have been performed at the LHVP (*Laboratoire d'Hygiène de la Ville de Paris*) station (48.829°N, 2.359°E), an urban background site in the center of Paris. EC concentrations are provided by an OCEC Sunset Field instrument at a resolution of one hour. The light absorption coefficient (at a measured wavelength of 637 nm, different from the instrument nominal wavelength of 670 nm) is measured by a Multi-Angle Absorption Photometer (MAAP, Model 5012, ThermoScientific[®]) at a 5 min resolution, and converted into EBC with a mass-specific absorption coefficient (MAC) of 8.8 m^2 g^{-1} derived from a linear regression between MAAP and OCEC Sunset measurements at the LHVP site (R^2=0.88, N=533, see Sect. S.1 in the Supplement, for details). NO_x observations come from a chemiluminescence monitor (AC31M, Environment SA) equipped with molybdenum oxide converters. However, an efficient conversion of many other nitrogen-containing compounds (NO_z=NO_y-NO_x) by the molybdenum converter can lead to interferences in the NO_x concentrations (Dunlea et al., 2007). This positive artefact varies from one location to the other, depending on the relative contribution of NO_z compounds in the NO_y family. Dunlea et al. (2007) have estimated a mean overestimation of +22% in Mexico city.

Among the chemical data available in the Paris plume, NO_y and EBC airborne measurements aboard the French ATR-42 aircraft have been used (see Freney et al., 2013, for a detailed description of the aircraft campaign). Measurements are available for several days in July: 1, 9, 10, 13, 15 (only EBC that day), 16, 20 (only NO_y), 21, 25, 28 (only EBC), 29 (only NO_y). NO_y concentrations were measured at a 30 s time resolution with an instrument designed for airborne measurements that

consists of three Ecophysics (CLD 780 TH) analyzers in which NO is measured using ozone chemiluminescence. NO_2 is photolytically converted, and NO_y is converted with H_2 in a gold covered heated oven (see Freney et al., 2013, for details). The limit of detection is 10 pptv. NO, NO_2 and NO_y measurement uncertainties have been estimated by these latter authors to 10, 20 and 20%, respectively. The measured NO_y includes the following species : NO, NO_2, HNO_2, HNO_3, HO_2NO_2, N_2O_5, PAN, PPN and particulate nitrate. EBC particles are collected with a 50% passing efficiency aerodynamic diameter of 5.0 μm (McNaughton et al., 2007), but most soot particles are likely in the fine mode. The light absorption coefficient is measured with a 60 s time resolution from the light absorption coefficient at 650 nm provided with a Particle Soot/Absorption Photometer (PSAP) instrument (Radiance research®), corrected as in Bond et al. (1999) (see Sect. S.2 in the Supplement for details). PSAP absorption coefficient measurement uncertainties are around 20-30% (Bond et al., 1999; Virkkula et al., 2005). Absorption values are then converted into EBC concentrations using the MAC of 8.8 m^2 g^{-1} already used at the LHVP site. The uncertainty related to the MAC is discussed in Sect. 4.3.4.

Various physical parameters are also measured in the ATR-42 aircraft at a 1 s time resolution including wind speed, wind direction and position of the aircraft (longitude, latitude, height). BL height (BLH) estimations are available at the SIRTA (*Site Instrumental de Recherche par Télédétection Atmosphérique*) (48.712°N, 2.208°E) (suburban background site at about 20 km in south-west of Paris) and LHVP stations. At SIRTA, they are estimated from ALS450 Leosphere backscatter lidar data at a 5 min time resolution (Haeffelin et al., 2012). At LHVP, values are estimated from CL31 ceilometer data (Haeffelin et al., 2012). Traditional meteorological parameters (wind, temperature) are also measured at SIRTA where, additionally, Leosphere wind cube lidar measurements are also available, providing wind measurements at a 10 min time resolution, each 20 m from 40 to 200 m above ground level (a.g.l.).

3.2 Emission inventories

Three European anthropogenic emission inventories are evaluated in this paper, all referring to year 2005:

1. The EMEP inventory (Vestreng et al., 2007), with a longitude-latitude resolution of 0.5° x 0.5°.

2. An inventory developed partly in the framework of MEGAPOLI project by TNO. The inventory for the year 2005 was constructed using official emissions submitted by European countries (downloaded from EEA in 2009) in combination with a gap-filling procedure using IIASA RAINS or TNO default data. The compiled emission data were spatially distributed at a resolution of $1/8^o$ x $1/16^o$ degree longitude–latitude (approximately 7 x 7 km). The development of the gridded data is described in Denier van der Gon et al. (2010) and Pouliot

et al. (2012). It is the year 2005 base case inventory and also serves as a starting point for the inventory described next. In this paper it is referred to as the TNO inventory.

3. A third inventory based on the TNO inventory and with the same $1/8^o$ x $1/16^o$ longitude–latitude resolution, but incorporating bottom-up emission data over the four European megacities (Paris, London, Rhine-Ruhr and Po valley). The city emission inventories were compiled by local authorities responsible for city emissions inventories and air quality such as Airparif for Paris (Airparif, 2010). It is described in more detail by Denier van der Gon et al. (2011), and has been previously used in Zhang et al. (2013) and Timmermans et al. (2013). It will be referred as the TNO-MP (MP for MegaPoli) inventory.

The same EC/OC speciation table, primarily associated to the TNO inventory, is applied in all inventories. Sector-dependent factors used to derive July emissions from annual ones are reported in Table S2 in the Supplement. This table also shows the total sectorwise BC July emissions over the region for the three inventories.

The resolution of both TNO and TNO-MP inventories is considerably improved compared to the EMEP inventory. Despite its coarse spatial resolution, the comparison of this latter inventory with the two other refined ones remains relevant for several reasons : (i) before being applied to simulations, emissions are downscaled to the air quality model resolution, here to a 3 km horizontal resolution, using the 1x1 km-resolved GLCF (Global Land Cover Facility) landuse database (Hansen et al., 2000; Hansen and Reed, 2000), and (ii) concentrations are considered in the Paris plume, i.e. at a rather large spatial scale, which decreases the influence of such a coarse resolution in the emissions. Emissions are apportioned according to several types of landuse : urban, rural, forest, crops and maritime (Menut et al., 2013). Because of their better horizontal resolution, the evaluation of emission inventories in this paper focused mainly on the TNO and the TNO-MP inventories, the EMEP is taken as an additional reference emission inventory, as it is used in many studies in Europe.

1
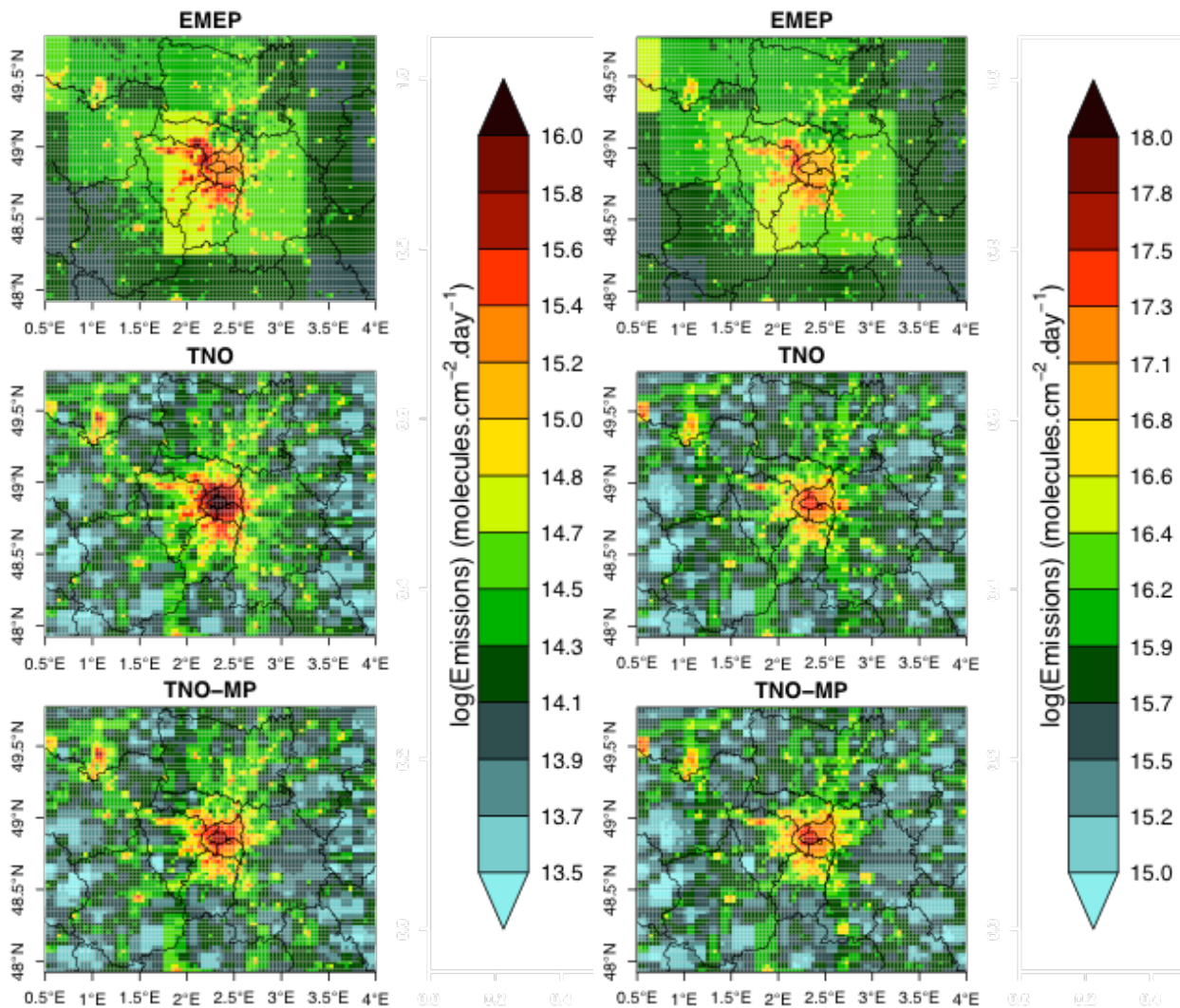
Figure 1 : BC (left panel) and NO$_x$ (right panel) emissions in EMEP, TNO and TNO-MP inventories.

The spatial distribution of BC and NO$_x$ emissions in the Paris region during a typical working day in July is given in Fig. 1 for each inventory. In order to illustrate the important differences in the spatial distribution of emissions between inventories, one can compute for all inventories the mean emissions of all cells within a certain distance around the LHVP site, from 0 (only the LHVP cell) to 80 km (the whole region) (see Fig. S3 in the Supplement). Relatively to TNO-MP, the EMEP inventory BC and NO$_x$ emissions in the Paris center are relatively low, but increase further away. The coarse resolution and the effect of the previously mentioned emission downscaling are clearly visible on Fig. 1 for EMEP emissions, and lead to obvious discontinuities between original cells. At a large scale, it gives the highest emissions for both compounds (and more particularly for NO$_x$ emissions). Conversely, TNO and TNO-MP inventories display significantly higher emissions in the agglomeration center, and lower ones further away. In summer, the TNO-MP inventory shows a quite similar spatial emission distribution as the TNO one. In particular, major highways around Paris, spatially unresolved or missing in the EMEP inventory, are clearly visible thanks to the refined resolution. However, BC emissions in TNO-MP are considerably lower than in TNO in the agglomeration. In absolute terms, discrepancies between both inventories mainly originate from road

1 transport (SNAP sector 7) and residential/tertiary (SNAP 2) sources, and in a lesser extent from

2 waste disposal (SNAP 9), non-road transport (SNAP 8) and industrial process (SNAP 4) sources (see

3 Table S2 in the Supplement for details). However, the highest relative discrepancies (that exceed a

4 factor of 3) are associated to SNAP 2, 8 and 9. For sources considered as area in the top-down TNO

5 inventory (e.g. SNAP 2 and 9), they are likely due to the distribution proxies used to downscale

6 national totals, leading to too high emissions in Paris where the population density is very strong

7 (Denier van der Gon et al., 2010). Concerning the SNAP 4 point sources, discrepancies can probably

8 be explained by the use of generic capacity rules in TNO, rather than exact emissions in the TNO-

9 MP. Both inventories are equivalent outside this region. A quite similar pattern is given for NO_x

10 emissions, except that discrepancies between both inventories in Paris are much reduced. In terms of

11 BC/NO_x emission ratios, highest values are given by the TNO inventory, followed by the EMEP one,

12 and finally the TNO-MP one. Differences are maximum in the center of Paris, and decrease when

13 integrating over larger areas.

14 It is worthwhile noting that as previously mentioned, both PSAP and MAAP instruments are based

15 on the measurement of the light absorption, and observations should thus be referred as EBC.

16 However, as emission factors and source profiles used to build emission inventories are mostly

17 expressed as EC (Vignati et al., 2010; Chow et al., 2011; Denier van der Gon, personnal

18 communication), the simulated "BC" should be regarded as EC. An ambiguity therefore arises from

19 comparisons between observed EBC and modeled EC since they correspond to different quantities.

20 This point is discussed in Sect. S.1 in the Supplement and in Sect. 4.3.4. In the following, the term

21 BC will be kept for convenience for both observations and simulations.

22 **3.3 CHIMERE model description**

23 In this paper, all simulations are performed with the CHIMERE CTM (Schmidt et al. 2001;

24 Bessagnet et al., 2009; Menut et al. 2013) (www.lmd.polytechnique.fr/chimere). The model was

25 originally designed to provide (i) short-term predictions of ozone and aerosol concentrations and (ii)

26 long-term (several years) predictions associated to emissions control scenarios. Besides research

27 activities, it allows operational air quality survey and forecasting, and is used by different local air

28 quality agencies in France (AASQA) and abroad, and by the French organization INERIS for daily

29 air quality forecasting in France and Europe (PREVAIR service, www.prevair.org). At European

30 scale, it is also used within the Copernicus GMES-MACC program.

31 The CHIMERE model allows simulating transport, gas-phase chemistry, some aqueous-phase

32 reactions, size dependent aerosol species including secondary organic aerosol, dry and wet

33 deposition. It treats coagulation, absorption as well as nucleation aerosol processes. Inorganic aerosol

34 thermodynamic equilibrium is calculated using the ISORROPIA model (Nenes et al., 1998).

3.4 Model configuration and simulated cases

In this paper, simulations are performed during the summer MEGAPOLI campaign (July 2009) with a five-day spin-up period. Two nested domains of increasing resolution — CONT3 (0.5 x 0.5°, i.e. ~50 x 50 km, 67x46 cells) and MEG3 (0.04 x 0.027°, 120x120 cells) — are considered (see Fig. S4 in the Supplement). The choice of the domains was previously explained in Zhang et al. (2013). The domain is subdivided into eight vertical layers, from ground to more than 5000 m height, with vertical resolution decreasing with altitude. The first three layers have a depth of about 40, 70 and 110 m, respectively.

Boundary and initial conditions are taken from LMDz-INCA2 global model for gaseous species and LMDz-AERO for particulate species (Hauglustaine et al., 2004; Folberth et al., 2006). The model uses the previously described anthropogenic emission inventories, while biogenic emissions are computed with MEGAN data and parametrizations from Guenther et al. (2006). In order to investigate the influence of meteorology on results, two meteorological dataset are considered. The first has been produced with PSU/NCAR Mesoscale Meteorological model (MM5; Dudhia, 1993), performed over three nested domains with increasing resolutions of 45, 15 and 5 km respectively, and using Global Forecast System (GFS) data from the National Center for Environmental Prediction (NCEP) as boundary conditions and large scale data. The second one has been produced with the Weather Research and Forecasting model (WRF; Skamarock et al., 2005; wrf-model.org) for the same domains and resolutions. Note also that MM5 and WRF have distinct boundary layer schemes : Medium Range Forecast (MRF) for the first, and Yonsei University (YSU) for the second.

4 Results and discussion

In this section, we first evaluate meteorological input data (Sect. 4.1). A first simple approach is then applied to evaluate BC emissions against NO_x ones, based on ground based measurements at the urban background LHVP site in Paris (approach n°1, Sect. 4.2). We then describe the procedure to evaluate BC emissions based on airborne measurements in the Paris plume, and present the corresponding results (approach n°2, Sect. 4.3). We finally discuss discrepancies between both methods (Sect. 4.4).

Statistical metrics are defined as :

- Mean bias: $MB = \dfrac{1}{n}\sum_{i=1}^{n}(m_i - o_i)$

$$(1)$$

- Normalized mean bias: $NMB = \dfrac{1}{n}\sum_{i=1}^{n}\dfrac{(m_i - o_i)}{\bar{o}}$

$$(2)$$

- Root mean square error: $RMSE = \sqrt{\dfrac{1}{n}\sum_{i=1}^{n}(m_i - o_i)^2}$

$$(3)$$

1   •   Normalized root mean square error: $NRMSE = \dfrac{1}{\bar{o}}\sqrt{\dfrac{1}{n}\sum_{i=1}^{n}(m_i - o_i)^2}$ (4)

2   •   Correlation coefficient: $R = \dfrac{\sum_{i=1}^{n}(m_i - \bar{m})(o_i - \bar{o})}{\sqrt{\sum_{i=1}^{n}(m_i - \bar{m})^2 \sum_{i=1}^{n}(o_i - \bar{o})^2}}$ (5)

3   Where m_i and o_i are the modeled and observed concentrations at time i, respectively, and $\bar{m}$

4   and $\bar{o}$ their averages over the period.

5   **4.1   Evaluation of meteorological data**

6   In this section, meteorological input data used in CHIMERE simulations, with both MM5 and WRF

7   models, are evaluated against observations at surface and in altitude.

8   **Surface observations.** The Fig. 2 shows comparisons between observations and simulations for

9   meteorological parameters obtained at the SIRTA ground site. Statistical results are reported in the

10   Table 1, considering all hours as well as only the 06:00-14:00 UTC time period (designed hereafter

11   as morning hours), more relevant in our methodology since transport from the urban emission

12   sources to the aircraft location occurs in the morning and the early afternoon.
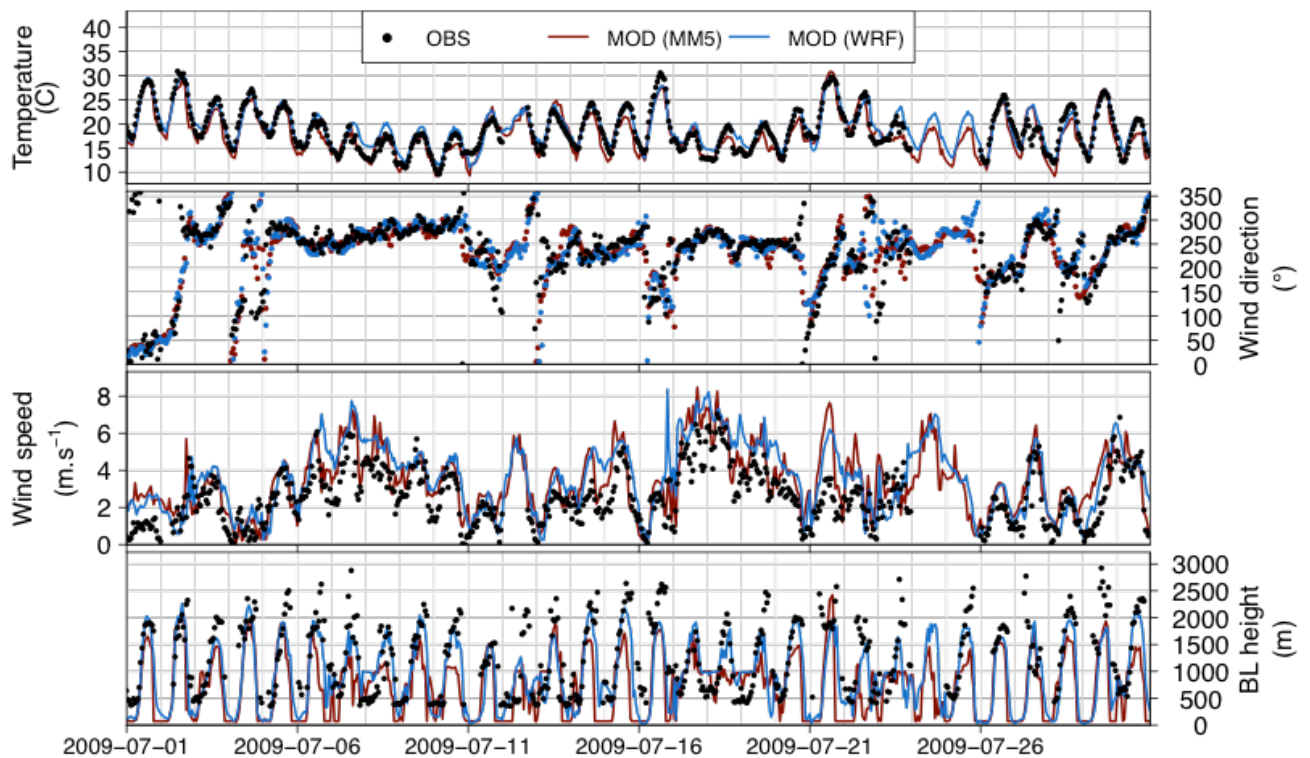
13

14   Figure 2 : Wind (at 10 m), temperature (at 2 m) and BLH time series in July 2009 at SIRTA site.

15   Except the first days of a continental north-easterly wind regime, the period is dominated by an

16   oceanic regime with west and south-west winds. The MM5 model shows a negative bias of -0.87°C

17   for ground temperature (reduced to -0.45°C by considering only morning hours), and a positive one

18   on wind speed (+33%). BLH appears strongly underestimated, with a bias of -34%, reduced to -24%

1 during morning hours. Satisfactory correlations are found for temperature (due to diurnal cycle) and

2 wind speed (R around 0.8-0.9), but lower ones are obtained for BLH (around 0.5). Conversely, the

3 WRF model shows better results on temperature (now slightly overestimated, with a bias of +0.45°C)

4 and overall BLH with an underestimation reduced to -17% (and -12% during morning hours).

5 Correlations on this latter parameter are significantly improved compared to MM5 model (0.7 against

6 0.5). As one of the factors contributing to the BLH negative bias, diurnal profile comparisons (see

7 Fig. S5 in the Supplement) show that the transition from a convective to a stable BL in the evening

8 hours occurs much too early in the MM5 model, particularly at the LHVP site. This shift carries on

9 with WRF but is seriously reduced, which explains the better correlations.

10 Table 1 : Statistical results of MM5 (and WRF in parenthesis) considering all July hours and only the

11 06:00-14:00 UTC time window (N represents the proportion of available data).

| Time range	Parameter	MB	NMB (%)	RMSE	NRMSE (%)	R (/)	N (%)
	Temperature (°C)	-0.87 (+0.45)	-	1.94 (1.57)	-	0.92 (0.94)	90
All hours	Wind speed (m s^{-1})	+0.83 (+0.99)	+33 (+39)	1.35 (1.47)	53 (58)	0.78 (0.80)	90
	BLH (m)	-440 (-224)	-34 (-17)	769 (553)	59 (43)	0.50 (0.69)	76
	Temperature (°C)	-0.45 (+0.29)	-	1.76 (1.60)	-	0.92 (0.94)	89
6:00-14:00 UTC	Wind speed (m s^{-1})	+1.04 (+0.71)	+35 (+24)	1.46 (1.18)	49 (39)	0.79 (0.84)	89
	BLH (m)	-345 (-176)	-24 (-12)	657 (530)	46 (37)	0.52 (0.65)	88

12

13 **Observations in altitude.** Wind lidar observations are compared with simulated wind speed in the

14 first model layers (the first vertical layers in CHIMERE are at 43, 118 and 248 m a.g.l.) (see Fig. S6

15 in the Supplement). Due to a low vertical resolution in simulations, comparisons remain qualitative.

16 MM5 and WRF models show quite similar patterns, but the MM5 model tends to give a higher wind

17 speed at all levels, including at ground. Statistical results over the 06:00-14:00 UTC time window in

1 the 110-210 m altitude range and for the flight days are reported on Table S3 in the Supplement. In

2 average, low negative biases and reasonable NRMSE are obtained with both MM5 and WRF models.

3 At the daily scale, biases on wind speed remain below ±30%, except the 13, 16 and 28 July

4 (respectively the 29 July) during which one or both models give high underestimations (respectively

5 overestimation), up to -46% (respectively +27% with MM5). Errors in terms of NRMSE exceed 25%

6 for all these dates, as well as during the 21 July (above 26%) despite a low bias (error compensation

7 between an underestimation during the first hours and overestimation during the last hours).

8 Wind speed simulation results are much better along the aircraft path (not shown), all biases

9 remaining below ±20% while NRMSE range between 12-32%. The highest biases occur the 1 and 28

10 July, around -18%. From a general point of view, the moderate positive bias found on wind speed at

11 ground vanishes in altitude except at mid-altitude during specific days, leading to a noticeable

12 decrease of the NRMSE.

13 **4.2   Approach n°1 : emissions evaluation from surface measurements**

14 BC emissions can be first evaluated at ground relatively to those of NO_x, by assuming that both

15 concentrations are proportional to their emissions close to their sources. Urban background BC and

16 NO_x concentrations, their ratio and their diurnal profiles are presented in Fig. 3, considering only

17 flight days. Details on the evaluation of CHIMERE against observations and statistical results are

18 given in Sect. S.3 in the Supplement. In a few words, BC is strongly overestimated, in particular with

19 the TNO inventory and during BL transitions, the use of WRF reduces biases mainly during the late

20 afternoon (after 18:00 UTC). NO_x is also overestimated, but mainly during the end of the day.

21 Observed BC/NO_x ratios are rather constant (0.06 µg m^{-3} ppb^{-1} in average) in July except during

22 some nights, but with a diurnal pattern showing lower values around 5 UTC and higher ones around

23 midnight. CHIMERE also simulates rather constant ratios but with a positive bias with TNO and to

24 less extent in EMEP inventories, while bias with TNO-MP emissions is rather small (< 13%).
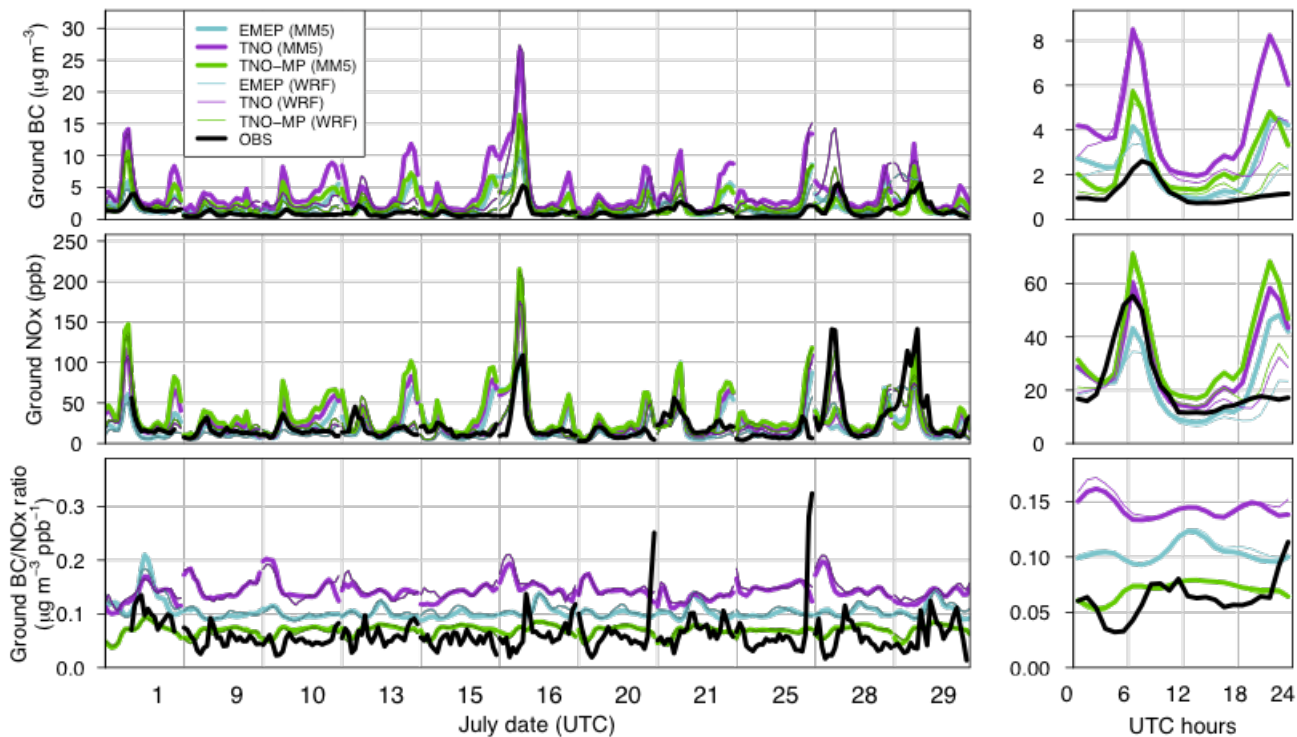
Figure 3 : BC and NO_x concentrations and BC/NO_x ratio at LHVP urban background site during July flight dates (left panel) and associated diurnal profiles (right panel).
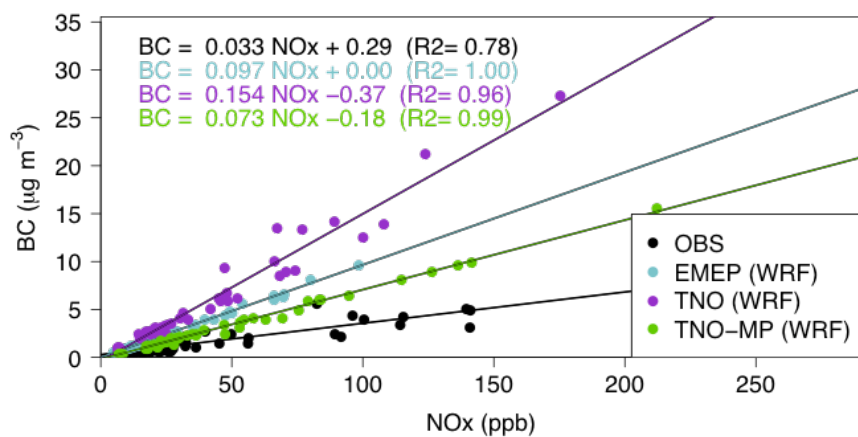
Figure 4 : Observed and simulated BC versus NO_x concentrations at LHVP between 05:00-08:00 UTC considering July flight days, and linear fits (lines). Only simulations with WRF meteorological data are reported here.

We now evaluate in some more detail BC emissions relatively to NO_x ones. In order to be comparable with the airborne approach, only flight days are considered, but some results over the whole month of July will also be indicated. It is worthwhile noting that, even if both BC and NO_x are mainly locally emitted within the Paris agglomeration, biases may be partly related to errors in advected contributions: BC can be transported from outside (like on July 1), while some NO_x may be

1　advected during the night and the early morning (when its photolytic conversion into HNO_3 or

2　HONO is less active) or released by reservoir species (e.g. PAN). NO_x measurements at two rural

3　background stations in the south and south-east of Paris are available from the AIRPARIF network.

4　In average, the NO_x regional background roughly accounts for 15-25% and 15-30% of the levels in

5　Paris for observations and simulations, respectively. From one year measurements during the

6　PARTICULES campaign (Bressi et al., 2013), it has been found that the BC regional background

7　contributes to about a third to the annual BC urban background average in Paris, and that this fraction

8　is probably underestimated by the CHIMERE model (Petetin et al., 2013). However, this uncertainty

9　source remains difficult to quantify more precisely. Additionally, NO_x chemiluminescence

10　measurements may also include some NO_z compounds (Dunlea et al., 2007), but this is not likely a

11　large error source since the CHIMERE model gives an average NO_x/NO_y ratio above 92% at the

12　LHVP site.

13　Given all these elements, we thus consider the BC/NO_x ratio over the 05:00-08:00 UTC time

14　window, corresponding to rush hours where fresh NO_x and BC are expected to dominate. BC versus

15　NO_x concentrations during that time window are represented in Fig. 4. Simulated slopes of BC versus

16　NO_x reported in Table 2 show a high overestimation with respect to observed ones for the TNO

17　inventory, around a factor of 4. Overestimations are reduced to a factor of 2.8 and 2.2 for EMEP and

18　TNO-MP inventories, respectively. Uncertainties on emission error factors (at a 95% confidence

19　interval) are quite the same for all inventories, around 18%, since they essentially originate from the

20　uncertainty on the slope deduced from observations (i.e. BC/NO_x ratios are more variable in

21　observations than in simulations). Note also that discrepancies between BC versus NO_x slopes and

22　BC/NO_x ratios (for the latter biases remain below +136%) are due to the diurnal variability of the

23　measured BC/NO_x ratio that shows the lowest values during the 05:00-08:00 UTC time window.

24　Results finally indicate an overestimation of BC emissions relative to NO_x emissions, particularly in

25　both top-down inventories (EMEP and TNO), that is significantly reduced with local bottom-up

26　information integrated in the TNO-MP inventory. It is worthwhile noting that, as a burning process-

27　related species of long lifetime, carbon monoxide is another appropriate candidate for the evaluation

28　of BC emissions (Zhou et al., 2009). However, it should also be mentioned that, due to its significant

29　background concentrations, higher uncertainties (compared to NO_x) may arise from errors in the

30　simulation of the regional background around Paris, even considering only rush hours.

31　Table 2 : BC versus NO_x slopes and emission error factors over the 05:00-08:00 UTC time window.

Case	Flight dates		All July dates	
	BC versus NO_x (µg m^{-3} ppb^{-1})	Model/observations ratio [uncertainty*]	BC versus NO_x (µg m^{-3} ppb^{-1})	Model/observations ratio [uncertainty*]

|					
MM5	EMEP	0.093±0.003	2.82 [18%]	0.095±0.001	2.79 [11%]
	TNO	0.135±0.009	4.09 [19%]	0.128±0.005	3.76 [11%]
	TNO-MP	0.075±0.002	2.27 [18%]	0.074±0.001	2.18 [11%]
WRF	EMEP	0.097±0.002	2.94 [18%]	0.097±0.001	2.85 [11%]
	TNO	0.154±0.010	4.67 [19%]	0.140±0.006	4.12 [11%]
	TNO-MP	0.073±0.002	2.21 [18%]	0.072±0.001	2.12 [11%]
Observations		0.033±0.006	-	0.034±0.004	-

1   * At a 95% confidence interval.

2

3   4.3   Approach n°2 : emissions evaluation from airborne measurements

4   Given these first results obtained at ground, the alternative approach based on airborne measurements
5   in the plume is now presented. The procedure is first described in details, and the results are then
6   shown and their uncertainties discussed.

7   4.3.1   Procedure to compute emission error factors (EEF)

8   As an illustration, the TNO/MM5 case for two flights on the 10 and 13 July are considered. Aircraft
9   trajectories and BC concentrations during these days are presented in Fig. 5. As previously
10   mentioned, the inlet used to collect BC particles is characterized by a 50% passing efficiency
11   aerodynamic diameter of 5.0 μm, and BC measurements are thus compared to the simulated BC
12   concentration below 5 μm. Time series given in Fig. 6 show a series of peaks that correspond to
13   successive crossings of the plume (time series for all July flights are given in Fig. S7 in the
14   Supplement). In both observations and simulations, the Paris region plume is well distinguishable
15   against background, and peaks can thus be located on the trajectory, giving the approximate central
16   line of the plume. Errors in the simulated wind direction lead to a shift in the spatial localization of
17   the plume (e.g. 13 July). It is worthwhile noting that some plumes from other cities may sometimes
18   be sampled by the aircraft. The case of the 13 July is notable: slight increases in BC concentrations in
19   the western part of the flight track (after 13:00 UTC) correspond to plumes from Rouen and Le
20   Havre, two industrial cities.

1
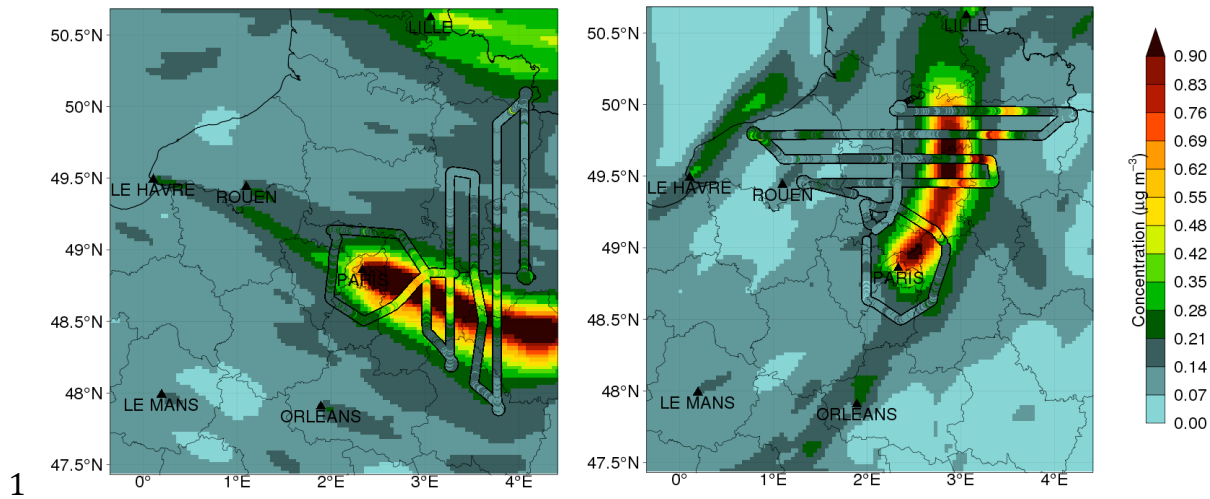
2 Figure 5 : Observed (along the aircraft trajectory) and modeled (in background, with the TNO-MM5
3 case) BC concentration for July 10 (left panel) and 13 (right panel). Paris and some other large cities are
4 indicated. Simulated concentrations shown here are taken at 13:00 UTC on the 4th layer that roughly
5 corresponds to 470-870 m height. The solid black line corresponds to the flight path outside that layer
6 (altitude above 870 m or below 470 m).
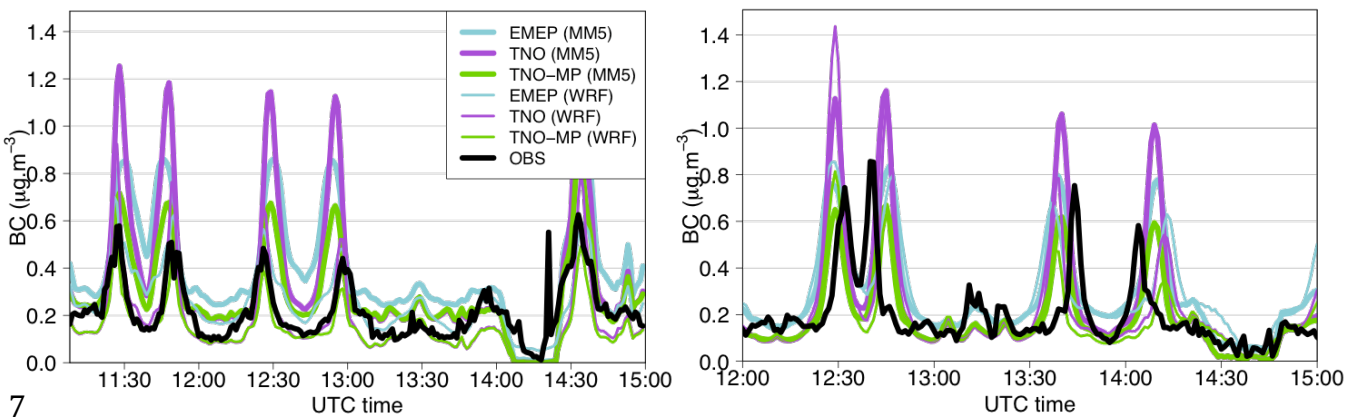
7

8   Figure 6 : Observed (in black) and simulated BC concentrations along the aircraft trajectory for July
9   10 (left panel) and 13 (right panel).

10   Concentration variations at the end of the flight correspond to a vertical profile up to 3 km a.g.l.
11   performed by the aircraft. We focus in this study on the time period during which the aircraft altitude
12   is rather constant (about 600 m a.g.l.). As briefly described in Sect. 2, the methodology consists in
13   computing for each transect the plume integral of concentrations above background, this latter being
14   estimated in both model and observations as the 30 percentile of concentrations in one transect (see
15   Fig. S8 in the Supplement). Only points above the background value are taken into account, and
16   additionally, some adjustments are made when winds bring plumes from other cities close to the
17   Paris one.

18   Given that the aircraft does not exactly cross the plume perpendicularly, but with an angle α between
19   0 and 90° that may be different in simulations compared to real world, a correction factor of sin(α) is
20   thus computed and applied to each peak area. Considering that atmospheric diffusion theories predict

1 a linear relationship between point source emissions and concentrations in the plume, an emission

2 error factor is finally defined for each flight as the ratio of the simulated area over the observed one

3 (i.e. an error factor of two means an emission overestimation of 100%).

4 The emission error factor is finally defined as :

$$EEF_{flight} = \frac{\sum_{peak} \sin(\alpha_{mod,peak}) \int_{peak} \left(C_{mod}(t) - C_{mod,background} \right) dt}{\sum_{peak} \sin(\alpha_{obs,peak}) \int_{peak} \left(C_{obs}(t) - C_{obs,background} \right) dt} \qquad (6)$$

6 It is worthwhile noting that such an evaluation applies to the combination of : (i) the PM emission

7 inventory, (ii) the PM speciation into BC, (iii) the monthly emission factor for July and (iv) the

8 hourly emission profile. If uncertainties are expected to be larger on the two first elements, the two

9 others may also contribute to the errors. In the following discussion, it is to be kept in mind that the

10 reference to BC emissions aggregates all these elements.

11 **4.3.2   Results on emission error factors**

12 BC and NO_x emission error factors are given for each flight on Fig. 7. Average results and

13 confidence intervals are also reported, considering errors as multiplicative:

14 • Mean : $\overline{EEF} = \exp\left(\frac{1}{n} \sum_{flight=1}^{nflights} \ln\left(EEF_{flight} \right) \right)$ (7)

15 • Confidence interval on the mean: $\sigma_{\overline{EEF}} = \exp\left(\frac{2}{\sqrt{n}} \sqrt{\frac{1}{n} \sum_{flight=1}^{nflights} \left(\ln\left(EEF_{flight} \right) - \ln\left(\overline{EEF} \right) \right)^2} \right)$ (8)

16 **BC and NO_x emissions evaluation.** Mean BC emissions results are quite contrasting between

17 inventories and suggest in average a slight overestimation of the EMEP inventory (+9% with MM5

18 data), a large overestimation of the TNO inventory (+45%) and an underestimation of the TNO-MP

19 inventory (-18%). Results on NO_x inventories show an overestimation ranging between +29 and

20 +39% depending on the inventory. As previously mentioned, NO_y measurements may include a part

21 of nitrate aerosols, but including them in the model has a very slight influence on results (NO_x mean

22 error factor changes remain below 11% for all inventories). Despite some discrepancies on specific

23 days between MM5 and WRF results, both give rather similar average emission biases. However, due

24 to the strong variability from one day to the other, uncertainties on these average values are high for

25 all inventories and both species, with a factor of about 1.39-1.47 for MM5 cases (at a 95%

26 confidence interval) but reduced to 1.27-1.31 for WRF simulations.

1
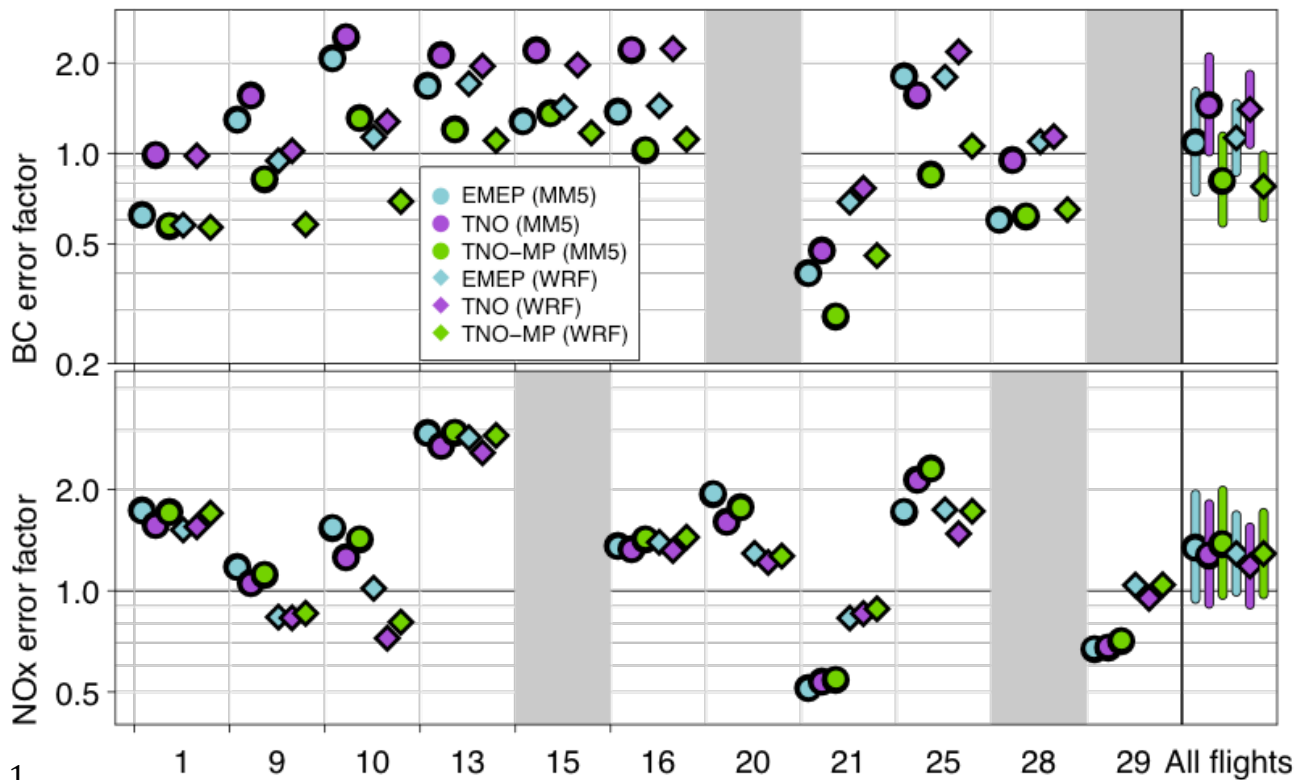
2   Figure 7 : BC (top panel) and NO_x (bottom panel) emission error factors for each individual flight

3   (when available) and averaged emission error factor (on the right) with 95% confidence interval, for

4   all six simulated cases (logarithmic scale).

5   **BC/NO_x emission ratio evaluation.** Ratios of BC emission error factors over NO_x ones are shown in

6   Fig. 8 (results considering all flights are reported in Table S4 in Supplement). On average, ratios

7   appear underestimated in EMEP and TNO-MP inventories (-18 and -46%, respectively), while a very

8   low EEF (+7%) is found for the TNO inventory. However, the day-to-day variability remains as high

9   as that of BC and NO_x taken individually, with an uncertainty on the mean around a factor 1.31-1.41.

10   In particular, rather small BC/NO_x error factor ratios are obtained the 1, 13 and 21 July (and the 25

11   with MM5 meteorology), compared to the other days.
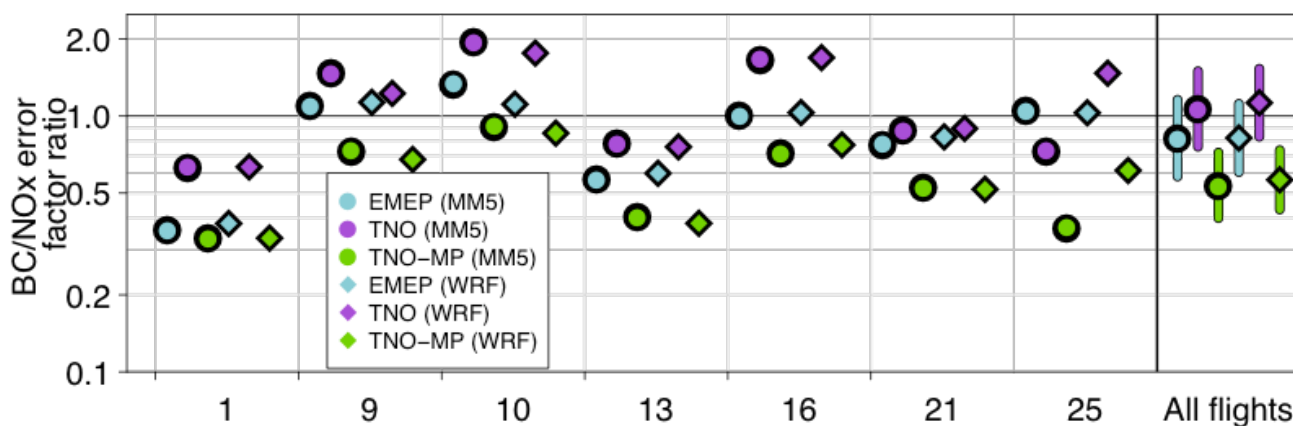
12

13   Figure 8 : BC/NO_x emission error factors ratio for each individual flight and averaged for all flights

14   (on the right) with confidence interval, for all six simulated cases (logarithmic scale).

Such a high day-to-day variability both in individual compounds EFF and in their ratio was not expected, which raises the question of its origin: does it come from the real-world emissions (missing in the model emission input data), or is it induced by uncertainties in the methodology, or both? In the next subsection, the variability potentially associated to observations themselves is discussed, while the variability that may come from the methodology (e.g. model errors) will be investigated in Sect. 4.3.4.

4.3.3 Variability in observations

When investigating ratios of the BC area over NO_y area for observations and simulations separately (see Fig. S9 in Supplement), one can notice that whatever the inventory, simulated BC/NO_x ratios remain rather constant from one flight to the other, leading to small uncertainties on the average value. Conversely, ratios derived from observations are much more variable, with higher values the 1, 13 and 21 July compared to other days (ratios above 0.15 against 0.06-0.09, i.e. close to a factor of 2), which induces uncertainties on the BC/NO_x average value in the same order of magnitude than those obtained on BC and NO_x separately. The model fails to reproduce such an enhancement during those days. The reasons for such an increase are not clear, but we can discuss some possible sources of variability.

Regional background heterogeneity. On July 1, BC measurements around Paris (and notably upwind of the city) show rather high but noisy concentrations (see Fig. S10 in Supplement), which suggests a possible heterogeneity in the BC regional background. In our methodology, a unique regional background value is estimated, based on the whole flight. In the case of a rather slender BC plume coming from the north in the axis of the Paris and adding itself to the city plume, our procedure would thus not be able to discriminate both. This may explain the high BC/NO_y ratio observed on that day.

Time window of emission sampling. Another possible source of variability in the BC/NO_x emissions is related to the time window of emission sampling, as BC/NO_x diurnal profiles at LHVP show lower values during morning rush hours than in the end of the morning (~0.04 against ~0.07 µg m^{-3} ppb^{-1}; see Fig. 3), with a noticeable day-to-day variability (see Fig. S11 in Supplement). The Paris plume sampled by the plane in the early afternoon at a distance up to 100 km from the city center originates from prior emissions, over different time windows depending on the wind speed. In order to assess which emissions are sampled in each flight, a new simulation case is run with the MM5 meteorology during the July month with 16 tracer compounds emitted each hour in a cell in the center of Paris, from 00:00 to 16:00 UTC. These inert compounds are only advected and deposited on the ground. By interpolating their concentration along each flight path, it is possible to compute the contribution of emissions at a specific hour to the overall plume. The Fig. 9a gives an illustration for July 28, for which observed wind speed at higher levels (110-210 m a.g.l.) is among the lowest (3.8

1 m s^{-1}, see Table S3 in Supplement). Tracer emissions follow a working day emission profile. Early

2 morning emissions of the day (in cold colors) dominate the two last peaks, while the latter emissions

3 contribution (in green and hot colors) progressively increases in earlier peaks. The contribution of

4 emissions at a specific hour is given by the integral ratio of the associated tracer concentration over

5 the total concentration (black area on the figure). On this flight, the aircraft thus sample emissions

6 over a quite large time window (00:00-11:00 UTC), with main contributions originating from 05:00-

7 07:00 UTC emissions (that account for 50% of the total area). The procedure is repeated for each

8 flight, and contribution results for all flights are presented on Fig. 9b, colored according to their

9 average wind speed in altitude (Table S3 in Supplement). Due to the large daily wind speed

10 variability, sampling is quite different from one flight to the other. Largest windows (00:00-11:00

11 UTC) are sampled during the 13, 16 and 28 July flights, for which wind speed remains quite low.

12 Most of other flights (1, 9, 10, 20, 25 July) with intermediate wind speed have a sample window

13 around 06:00-11:00 UTC, while the strongest wind speeds occurring the 15 and 21 July lead to

14 sampling of 09:00-12:00 UTC emissions. As only late emissions are sampled on July 21, this may

15 explain higher ratios obtained in the plume. Unfortunately, no NO_y measurements are available the

16 15 July with similar high wind speeds to confirm such a tendency. However, that explanation does

17 not apply to the 13 July flight (large window) for which the high ratio thus remains unexplained.

18 Note that the use of WRF is not expected to substantially modify the results obtained here with MM5

19 since major discrepancies between both meteorological model outputs only concern the BLH starting

20 from 10:00 UTC and that emission tracers are here investigated relative to each other.

21 (a)   (b)
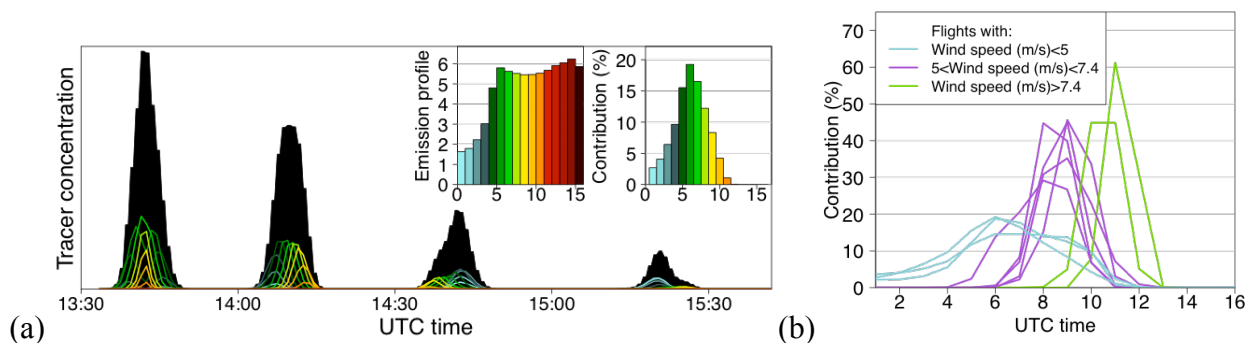
22 Figure 9 : (a) Concentration along the flight trajectory of the 16 tracers (in color line) and their total

23 (in black) during the 28 July flight. The emission profile gives the color associated to each tracer as

24 well as their emission intensity. The hourly emissions contribution over all peaks of each tracer to the

25 total (in terms of area) is shown in the top right corner. (b) Hourly emissions contribution to total area

26 for all flights. At each flight corresponds a line colored according to the mean wind speed in altitude

27 given in Table S3 in the Supplement. Note that, as flights occur in the afternoon, only the 16 first

28 hours of the day are represented.

4.3.4 Uncertainties of the inversion methodology

The methodology used to evaluate NO_x and BC emission inventories based on aircraft data over the Paris region intends to minimize several error sources : (i) the representativeness error by considering concentrations in the plume rather than at ground, (ii) modeled chemistry errors by considering inert tracer species/families, and (iii) lateral dispersion and plume direction errors by considering integrated concentrations. The high emission error factors day-to-day variability previously noticed is partly due to a variability in Paris agglomeration emissions, but such large discrepancies are not expected, and are indicative of other uncertainty sources that must be at stake, among which : (i) the wind field errors and their impact on emissions really sampled by the plane, (ii) errors in BLH and vertical mixing, (iii) errors in deposition, and finally (iv) discrepancies between EBC and EC. All these uncertainty sources are investigated in this section. Overall emission error factors uncertainties are then discussed in Sect. 4.3.5.

Wind speed and emission profiles. The methodology does not evaluate annual monthly emissions alone but also a part of the applied diurnal emission profiles (see Sect. 4.3.3) and errors on wind speed may shift the time window over which emissions are sampled (in simulations with respect to reality). This causes an additional uncertainty all the more important that the time window is narrow and temporal emission gradients are strong. In addition, wind speed errors within the city directly determine the residence time of air masses close to emission sources and thus the degree of pollutant accumulation.

Significant wind speed NRMSE at the SIRTA site, both at ground and at altitude levels below 200 m a.g.l. (around 40-60% and 10-60%, respectively), have been found (Sect. 4.1). These errors influence the accumulation of emitted pollutants within the city, for which uncertainties are thus probably quite important, as the accumulation time is at first order inversely proportional to the wind speed. Thus, this uncertainty in the local wind speed appears as an important source of uncertainty and variability in the day to day emission error factors. On the contrary, biases in the wind speed are reasonable, for example mostly below ±30% for the wind speed at SIRTA between 100 and 200 m a.g.l., thus indicating no particular bias in emission error factors due to this error source.

Another uncertainty source is related to wind speed errors at higher altitudes (between the agglomeration and the measurement location), and subsequent errors on the plume advection. Given the diurnal profile of emissions and the variable emission time window sampled by the plane depending on the wind speed (Sect. 4.3.3), an error on advection would shift this time window toward earlier (respectively later) emissions in case of negative (respectively positive) biases on wind speed in altitude. This error source thus appears all the more important that the gradient in the diurnal emission profile is high in the sampled time window. Daily biases on wind speed below ±20% have been found in airborne measurements along the flight path. If these uncertainties are taken as

1 representative for the average wind between the emission source and the aircraft, the typical

2 displacements of the emission time window are less than about 1h. This would induce significant

3 errors (say above 10%) only for time windows between 05:00 and 08:00 UTC, when the temporal

4 gradient in emissions is strong. Thus this error source should not be of major importance to explain

5 the variability in results.

6 **Vertical mixing.** As previously highlighted, aircraft measurements are expected to have a higher

7 spatial representativeness than at ground, but this relies on the assumption that the vertical mixing in

8 the BL is correctly established, so that observations obtained in the plane, at an altitude of about 600

9 m a.g.l., can be considered as representative of those in the whole plume. The vertical heterogeneity

10 is expected to be the highest above the city and to decrease gradually along the plume due to the

11 turbulent mixing and the absence (or the relatively poor contribution) of fresh emissions at ground

12 outside the city. The vertical turbulent mixing parametrization in the CHIMERE model follows the

13 K-diffusion approach of Troen and Mahrt (1986) without counter-gradient term. Vertical fluxes are

14 directly proportional to the vertical turbulent diffusivity coefficient (K_z) that is bounded in the model

15 by a minimum value of 0.01 and 1 m^2 s^{-1} in the dry and cloudy BL, respectively, and by a maximum

16 value of 500 m^2 s^{-1} (Menut et al., 2013). To assess the influence of vertical mixing on results, a

17 sensitivity test is performed by multiplying and dividing K_z values by two, as in Vautard et al.

18 (2003). Both the dry minimum and the maximum boundaries are kept in the sensitivity test. Relative

19 changes are shown in Fig. S12 in the Supplement. Dividing (respectively multiplying) the K_z by two

20 leads to a moderate increase below +19% (respectively a decrease below -16%) for BC and NO_x,

21 while the BC/NO_x ratio does not change by more than 6%. Such small changes are quite consistent

22 with the results obtained over the Paris agglomeration by Vautard et al. (2003) who explain the

23 moderate impact of K_z on concentrations in altitude by the fact that a larger diffusivity increases both

24 the incoming vertical flux from lower layers and the outgoing one toward higher layers.

25 **Boundary layer height.** The BLH is the other important parameter that requires to be correctly

26 modeled, since it determines the volume into which the emissions will be diluted within the plume.

27 During early afternoon, Lidar observations at SIRTA and LHVP sites have shown an underestimation

28 by MM5 model, while significant improvements are obtained with WRF model but still with a

29 negative bias at the SIRTA suburban site (Sect. 4.1). If such an underestimation exists in the whole

30 flight region, it may lead to an overestimation of emission biases. However, processes are not linear,

31 since the increased concentrations due to a lower BLH may for instance be reduced by a higher dry

32 deposition (that depends on concentrations in lowest level). In order to assess the importance of these

33 errors, a sensitivity test is performed with the EMEP/MM5 case by increasing the BLH by 30%

34 (corresponding to the mean bias between 06:00-14:00 UTC). So far, simulated cases have been

35 performed with prognostic turbulent parameters (i.e. directly taken from meteorological models).

36 However, as the diffusivity coefficient depends on the BLH, the sensitivity test with BLH multiplied

1   by 130% is performed with the diagnostic option, in which K_z is calculated within the CTM among

2   others as a function of the BLH. Except for some specific dates (10, 20 and 28 July), a larger BLH

3   leads to lower concentrations and therefore decreases error factors (see relative changes in Fig. S12

4   in the Supplement). On average, changes are around -14% for both BC and NO_x, and have rather no

5   influence on the mean BC/NO_x ratio (-1%). Thus, the uncertainty in BLH could both contribute to the

6   variability and bias in BC and NO_x emission error factors, while the BC/NO_x ratio is rather

7   unaffected by these errors.

8   **Deposition.** BC and NO_y are expected to be conservative at the time scale of the flight, but they both

9   undergo deposition. Errors in the simulated deposition and/or in the NO_y speciation (given the large

10   differences of deposition rates among NO_y individual compounds) may impact emission biases

11   results. Meteorological conditions indicate that wet removal is likely to be negligible over the

12   campaign region, and the deposition is thus essentially dry. In order to assess the influence of

13   deposition on results, a sensitivity test based on the EMEP/MM5 case is performed without any dry

14   or wet deposition. Relative changes on BC, NO_x error factors and on their ratios are reported on Fig.

15   S13 in the Supplement. Removing deposition increases all error factors by various amounts

16   depending on the day. On average, error factor changes on BC and NO_x are around +7 and +16%,

17   respectively. Without deposition, the BC/NO_x error factor ratio is decreased by -9% in average.

18   These figures are upper limits, as errors in deposition speed are most probably less than 100%. Thus,

19   uncertainty in deposition likely does not very much affect the error budget.

20   **Mass-specific absorption coefficient.** As previously mentioned, an additional uncertainty may arise

21   from the comparison between EBC (observations) and EC (emissions and simulations), through the

22   MAC value used to convert absorption coefficients into EBC concentrations. Airborne PSAP EBC

23   concentrations have been obtained considering a constant MAC of 8.8 m^2 g^{-1} deduced from

24   measurements at the LHVP site in Paris (see Sect. S.1 in the Supplement). The relevancy of

25   comparisons performed in this study with the simulated EC thus relies on the hypothesis that this

26   MAC determined in the Paris center is valid at the scale of the whole agglomeration, and that it

27   remains constant along the flight. This is supported by the MAC value estimated in winter 2009 by

28   Sciare et al. (2011) at a suburban site at 20 km in the south-west of Paris that remains in the same

29   order of magnitude than the one obtained here in the Paris center (7.3±0.1 m^2 g^{-1}). Actually, during

30   that winter season, but one year later, single particle Aerosol Time-Of-Flight Mass Spectrometer

31   observations performed at the LHVP site during the MEGAPOLI winter campaign have shown a

32   majority of already internally mixed BC particles (with a shell of organic material and secondary

33   inorganic compounds) (Healy et al., 2012). Therefore, the MAC variations along the flight are

34   expected to be reasonable. This is also supported by the analysis of BC/NO_y ratios obtained from

35   aircraft observations that does not show any significant increase with distance from Paris, which

36   would be expected if the MAC value increased with distance from the emission source. Additionally,

it is worthwhile noting that direct measurements of the MAC enhancement by Cappa et al. (2012) have recently shown a very low enhancement between near source and more distant values, only by around +6%, onboard a ship along the California coast (CalNex campaign) and at a ground site located at 14 km of Sacramento (Carbonaceous Aerosols and Radiative Effects Study, CARES campaign). Considering the previous MAC estimations in the Paris region — 7.3 and 12.0 m^2 g^{-1} by Sciare et al. (2011) and Liousse et al. (1993), respectively — the uncertainty associated to our MAC value (8.8 m^2 g^{-1}) is roughly estimated at 30%.

4.3.5   Statistical significance of the results

Results obtained for each compound in Sect. 4.3.2 consist in mean error factors and rather large confidence intervals that result from (i) uncertainties associated to the day-to-day variability which is not included in the model input data (beyond the temporal dependence on the month and the day of the week), (ii) measurement uncertainties and (iii) uncertainties in the methodology (conditioned by error sources in the model).

The first ones are difficult to quantify but can reasonably be considered as random. Also measurement uncertainties are probably mostly random, but may include a part of systematic uncertainties. In order to be conservative, they are assumed entirely as systematic. Uncertainties in the methodology have been discussed in previous sections, notably through various sensitivity tests on deposition, boundary layer height and the turbulence diffusivity coefficient. Results have shown that all investigated uncertainties in the model influence mean emission error factors, and their variability. They have therefore a systematic and a random part, which we could estimate in the previous sensitivity tests. These tests have shown a significant day-to-day variability, which suggests that they are probably partly random and may thus explain most of the day-to-day variability obtained in first results (Sect. 4.3.2). It appears rather tricky (and uncertain) to explain all discrepancies between individual flight results on a quantitative basis, notably due to the fact that several uncertainty sources are potentially combined. In spite of that, the choice is made to replace the uncertainty obtained in Sect. 4.3.2 by a combination of all the systematic uncertainties estimated in the previous subsection. Results of individual and the derived overall systematic uncertainty are reported in Table 3, as well as final confidence intervals on our estimation of emission error factors.

Table 3: Systematic two-sigma uncertainties on BC and NO_x error factors and BC/NO_x error factor ratio from various sources, and associated confidence intervals on average emission error biases for the three inventories.

Uncertainty source	BC	NO_x	BC/NO_x
Boundary layer height	14%	14%	1%

Vertical mixing	17%	19%	6%
Deposition	7%	16%	9%
Mass-specific absorption coefficient	30%	-	30%
NO_y and absorption coefficient measurement	30%	20%	36%
Overall uncertainty	48%	35%	48%

1   Confidence intervals (at a 95% confidence interval) on average emission error biases deduced from
2   the overall uncertainty are reported in Table 4. For NO_x emissions, positive biases are found in all
3   inventories. Considering the 95% confidence intervals, the bias in the TNO inventory appears
4   statistically insignificant, which may not be the case in both EMEP and TNO-MP inventories for
5   which a slight overestimation remains probable (due to a confidence interval lower bound of -4%,
6   thus very close to zero). These are in the range of the 35% agreement found for NO_x emissions in
7   Paris during the ESQUIF project in summer 1999 by Vautard et al. (2003) also based on airborne
8   measurements and CHIMERE simulations, but using an alternative method, and an older emission
9   inventory prepared by AIRPARIF. Through an inverse modeling exercise based on satellite NO_2
10   columns, Konovalov et al. (2006) have obtained a similar 30% overestimation of the EMEP
11   inventory in the Paris area. Through another inverse emission modeling based on ground
12   measurements over the Paris region, Deguillaume et al. (2007) have found no significative bias, but
13   an uncertainty of about ±20 %. Note that these studies were performed using different emission
14   inventories. Given the uncertainties, the NO_x emissions positive bias around 20-30% found here in
15   most of the inventories does not appear as significant.

16   Table 4 : Confidence intervals on average emission error biases for the three inventories.

Inventory	BC	NO_x	BC/NO_x
EMEP	+12% (-24%; +66%)	+29% (-4%; +74%)	-18% (-45%; +22%)
TNO	+40% (-6%; +108%)	+18% (-12%; +59%)	+13% (-24%; +67%)
TNO-MP	-23% (-48%; +15%)	+29% (-4%; +74%)	-44% (-62%; -17%)

17   Also both the positive bias (around +12%) of EMEP and the negative one (around -23%) of TNO-
18   MP BC emissions are not significant, while the 95% confidence interval of the TNO inventory
19   indicates a probable overestimation of BC emissions in that inventory. As previously mentioned in

1 Sect. 3.2, the overestimation of BC emissions in the TNO inventory can probably be explained by the

2 spatial distribution procedure that concentrates too large emissions in the city. For example, using

3 population density as a proxy implies the assumption of constant per capita emissions over the

4 country which might lead to an overestimation of urban BC emissions as discussed in Timmermans

5 et al., (2013) and references therein. At this stage, it is to be emphasized that discrepancies between

6 EMEP and TNO BC results are mostly related to differences in their spatial resolution since input

7 data for national totals are similar. Accordingly, Paris region total emissions in July are quite similar

8 in both EMEP and TNO inventories (as shown in Table S2 in Supplement). However, at the scale of

9 the Paris agglomeration, total emissions in both inventories do show discrepancies, TNO emissions

10 being more concentrated in the city due to its finer resolution while the EMEP emissions spill over in

11 rural areas of Paris region due to their coarser resolution (see Sect. 3.2). Therefore, to our sense, the

12 better results obtained with EMEP have to be interpreted with caution. Potential errors in the

13 distribution of BC emissions are partly avoided in the TNO-MP inventory which follows a more (but

14 not fully) bottom-up approach. Concerning the BC/NO_x emission ratio, the only statistically

15 significant negative bias concerns the TNO-MP inventory, while results for both EMEP and TNO

16 inventories suggest error compensation in BC and NO_x emissions, leading to a satisfactory estimation

17 of BC/NO_x emission ratio. It is worthwhile reminding that, in this study, the same BC speciation

18 table (primarily built for the TNO inventory) has been used in all inventories in order to be

19 consistent, but the use of a more specific speciation to the Paris region would maybe change these

20 results, in particular for the TNO-MP inventory in which a part of the bottom-up information is lost

21 through the use of a constant BC speciation in this study. Another point to be mentioned concerns the

22 emissions inter-annual variability that adds an additional uncertainty (similar for all inventories) due

23 to the comparison of observations from 2009 with inventories built for 2005.

24 To our knowledge, a BC emissions evaluation as presented here has not yet been attempted at the

25 scale of a large megacity, and uncertainties estimated at the global or regional scale are difficult to

26 extrapolate to an agglomeration. For comparison, through their adjoint inverse modeling exercise

27 over Asia, Hakami et al. (2005) have found quite consistent total assimilated and base case BC

28 emissions over Asia, but have underlined higher discrepancies at regional scale, with major errors

29 over Japan, northern and southern China of about a factor ± two.

30 **4.4 Surface versus airborne results : representativeness issues**

31 Results obtained at ground in Paris show a high overestimation of the BC/NO_x ratio in the TNO (~

32 factor 4) and EMEP (~ factor 3) inventories, and at a lesser extent in TNO-MP (~ factor 2). This is

33 not consistent with results obtained in the plume where the BC/NO_x emission ratio appears highly

34 underestimated in TNO-MP (while errors are lower for EMEP and TNO). Several reasons may at

35 least partly explain these discrepancies between ground and airborne results. The main one is

36 probably the difference of representativeness between both approaches, ground concentrations being

1   influenced by emissions in the vicinity of the LHVP station, while concentrations in the plume

2   integrate emissions at a much larger scale (the whole agglomeration). In order to assess the LHVP

3   site representativeness, a simulation with spatially traced emissions around that site is performed over

4   a few days (see Sect. S.4 in the Supplement). LHVP concentrations appear mainly influenced by

5   close emissions, with a contribution of 50-85% from emissions within a radius of 6 km around the

6   site. Conversely, beyond a radius of 21 km (which still covers the agglomeration), emissions

7   contribute to less than 10%. These contributions are quite variable depending on the wind field, the

8   importance of close emissions increasing with stagnant conditions. Since BC and NO_x emissions as

9   well as their ratio are highly heterogeneous over the whole Paris region (see Sect. 3.2 and Fig. S3 in

10   the Supplement), results obtained at the LHVP site thus cannot be representative for the whole

11   agglomeration, but probably only for its central part.

12   Additionally, the previous tracer experiment takes into account neither the sub-grid emissions

13   heterogeneity at a resolution of 3x3 km (e.g. a park and a stretch of the Paris ring road are included in

14   the LHVP cell) nor sub-cell processes, caused by the high complexity of urban environments (e.g.

15   street canyons, building-induced turbulence). The LHVP spatial representativeness may thus be even

16   lower. Working at the plume scale strongly reduces these limitations since (i) all emissions within the

17   agglomeration end up in the plume, and (ii) mixing during a few hours of transport from the source

18   regions to the measurement locations is expected to significantly increase the concentration

19   representativeness.

20   This would therefore suggest that the best BC/NO_x emission ratio is given by the TNO-MP inventory

21   in the Paris center, while it highly underestimates the ratio at the scale of the whole agglomeration,

22   contrary to the TNO inventory which gives better results. Compared to TNO-MP, NO_x emissions in

23   TNO are quite similar while BC ones are higher and more concentrated in the center of Paris.

24   **5   Conclusion**

25   Black carbon (BC) emissions are still highly uncertain, and very few studies have attempted to

26   evaluate their inventories. This paper presents an original approach, based on airborne measurements

27   across the Paris plume, developed in order to evaluate BC and NO_x emissions at the scale of the

28   whole agglomeration. It is applied to three emission inventories (EMEP, TNO, TNO-MP). In order to

29   assess the benefit of such a methodology, BC/NO_x ratios at the LHVP ground site in Paris are first

30   investigated. Over the whole July month, they show a significant (at a 95% confidence interval)

31   overestimation in all inventories with biases ranging between a factor of 2 in TNO-MP and a factor

32   of 4 in TNO. On average, results obtained from July airborne observations give an overestimation of

33   NO_x emissions around +20-30% for all inventories, a moderate bias around +12 and -23% for EMEP

34   and TNO-MP BC emissions, respectively, but a higher positive bias of +40% for TNO BC inventory.

35   However, these results present an unexpected high day-to-day variability (up to a factor of about 3).

Low biases are also obtained on BC/NOx emission ratio for EMEP and TNO inventories (-18 and +13%, respectively), contrary to the TNO-MP inventory that shows an underestimation of -44%.

Various uncertainty sources in the methodology are investigated through sensitivity tests — wind field errors, boundary layer height, vertical mixing, deposition, BC nature (equivalent BC versus elemental carbon) — and are likely to explain this variability. Results of these tests are used to derive a systematic uncertainty between 35 and 48% on emission error factors. This suggests that a moderate overestimation of NO_x July emissions in EMEP and TNO-MP inventories is statistically probable. Biases found in EMEP and TNO-MP BC emissions are not significant. However, the overestimation in TNO BC emissions does appear as significant. It is probably due to the distribution proxies used to downscale national total emissions that concentrate too large emissions in a highly populated area such as Paris with lower per capita emissions. The BC/NO_x emission ratio appears underestimated in the TNO-MP inventory, while non-significant biases are obtained with both EMEP and TNO inventories. While discrepancies between EMEP and TNO inventories are likely due to differences in spatial resolutions and allocation, the ones between TNO and TNO-MP do illustrate the distinction between bottom-up and top-down approaches. Results obtained at a ground based site in Paris are not consistent with those obtained in the plume, due to the fact that surface measurements are representative only for an area surrounding the LVHP site by a few kilometers while emissions from the whole agglomeration are sampled in the Paris plume.

Finally, best estimations of BC and NO_x emission biases thus do not exceed ±40%, which appears as rather moderate considering the numerous uncertainties at stake in the construction of an inventory. Due to methodological uncertainties in the same order of magnitude, assessing the significance of all these results remains difficult. However, the methodology does succeed in highlighting some statistically significant biases and in particular, for BC or NO_x emissions or for the BC/NO_x ratio, at least one of the three inventories has been proven as very probably biased. It is worthwhile noting that the methodology used in this study not only evaluates an inventory by itself but also a particulate matter speciation table and a temporal disaggregation (monthly and diurnal) that are also subject to potential errors.

To our knowledge, this study is one of the most comprehensive ones to evaluate BC emissions at the scale of a large megacity. The comparison of aircraft- and ground-based results has given an interesting insight on the potential error compensation in the spatial allocation of BC emissions over a large agglomeration. In the framework of the PRIMEQUAL PREQUALIF project, a dense BC network of 14 stations (of various typologies, e.g. rural, urban, traffic) has been installed over the Paris region. It will allow a better characterization of the BC spatial distribution over the agglomeration, and in the line of this, an interesting outlook would thus be to compare it to the simulated spatial distribution constrained by emission inventories.

References

Airparif : Inventaire des émissions en Ile-de-France, Méthodologie et résultats année 2005 (in french), 2010.

Baklanov, A., Lawrence, M., Pandis, S., Mahura, A., Finardi, S., Moussiopoulos, N., Beekmann, M., Laj, P., Gomes, L., Jaffrezo, J.-L., Borbon, A., Coll, I., Gros, V., Sciare, J., Kukkonen, J., Galmarini, S., Giorgi, F., Grimmond, S., Esau, I., Stohl, A., Denby, B., Wagner, T., Butler, T., Baltensperger, U., Builtjes, P., van den Hout, D., van der Gon, H. D., Collins, B., Schluenzen, H., Kulmala, M., Zilitinkevich, S., Sokhi, R., Friedrich, R., Theloke, J., Kummer, U., Jalkinen, L., Halenka, T., Wiedensholer, A., Pyle, J., and Rossow, W. B. : MEGAPOLI : concept of multi-scale modelling of megacity impact on air quality and climate, Advances in Science and Research, 4, 115–120, 2010.

Bessagnet, B., Menut, L., Curci, G., Hodzic, A., Guillaume, B., Liousse, C., Moukhtar, S., Pun, B., Seigneur, C., and Schulz, M. : Regional modeling of carbonaceous aerosols over Europe - focus on secondary organic aerosols, J. Atmos. Chem., 61, 175–202, 2009.

Bond, T. C., Anderson, T. L., and Campbell, D. : Calibration and Intercomparison of Filter-Based Measurements of Visible Light Absorption by Aerosols, Aerosol Sci. Tech., 30, 582–600, 1999.

Bond, T. C., Streets, D. G., Yarber, K. F., Nelson, S. M., Woo, J.-H., Klimont, Z.: A technology-based global inventory of black and organic carbon emissions from combustion, J. Geophys. Res., 109, D14 203, 2004.

Bond, T. C., Doherty, S. J., Fahey, D. W., Forster, P. M., Berntsen, T., DeAngelo, B. J., Flanner, M. G., Ghan, S., Kärcher, B., Koch, D., Kinne, S., Kondo, Y., Quinn, P. K., Sarofim, M. C., Schultz, M. G., Schulz, M., Venkataraman, C., Zhang, H., Zhang, S., Bellouin, N., Guttikunda, S. K., Hopke, P. K., Jacobson, M. Z., Kaiser, J. W., Klimont, Z., Lohmann, U., Schwarz, J. P., Shindell, D., Storelvmo, T., Warren, S. G., and Zender, C. S. : Bounding the role of black carbon in the climate system : A scientific assessment, J. Geophys. Res.-Atmos., 118, 1–173, 2013.

Bressi, M., Sciare, J., Ghersi, V., Bonnaire, N., Nicolas, J. B., Petit, J.-E., Moukhtar, S., Rosso, A., Mihalopoulos, N., and Féron, A. : A one-year comprehensive chemical characterisation of fine aerosol ($PM_{2.5}$) at urban, suburban and rural background sites in the region of Paris (France), Atmos. Chem. Phys., 13, 7825–7844, 2013.

Cappa, C. D., Onasch, T. B., Massoli, P., Worsnop, D. R., Bates, T. S., Cross, E. S., Davidovits, P., Hakala, J., Hayden, K. L., Jobson, B. T., Kolesar, K. R., Lack, D. A., Lerner, B. M., Li, S.-M., Mellon, D., Nuaaman, I., Olfert, J. S., Petäjä, T., Quinn, P. K., Song, C., Subramanian, R., Williams, E. J., and Zaveri, R. A. : Radiative absorption enhancements due to the mixing state of atmospheric black carbon, Science (New York, N.Y.), 337, 1078–1081, 2012.

Chow, J. C., Watson, J. G., Lowenthal, D. H., Antony Chen, L.-W., and Motallebi, N. : $PM_{2.5}$ source profiles for black and organic carbon emission inventories, Atmos. Environ., 45, 5407–5414, 2011.

Dallmann, T. R. and Harley, R. A. : Evaluation of mobile source emission trends in the United States, J. Geophys. Res., 115, D14 305, 2010.

Deguillaume, L., Beekmann, M., and Menut, L. : Bayesian Monte Carlo analysis applied to regional-scale inverse emission modeling for reactive trace gases, J. Geophys. Res., 112, D02 307, 2007.

Denier van der Gon, H.A.C., Visschedijk, A. van der Brugh, H. Dröge, R. : A high resolution European emission data base for the year 2005. A contribution to UBA-Projekt PAREST: Particle Reduction, Strategies, TNO-034-UT-2010-01895_RPT-ML, 2010.

Denier van der Gon, H.A.C., Beevers, S., Al D'Allura, et al. : Discrepancies between top-down and bottom-up emission inventories of megacities: the causes and relevance for modeling concentrations and exposure. In: Steyn, D.G., Castelli, S.T. (Eds.), NATO Science for Peace and Security Series C: Environmental Security, vol. 4, 2011.

Dudhia, J. : A Nonhydrostatic Version of the Penn State-NCAR Mesoscale Model : Validation Tests and Simulation of an Atlantic Cyclone and Cold Front, Mon. Weather Rev., 121, 1493–1513, 1993.

Dunlea, E. J., Herndon, S. C., Nelson, D. D., Volkamer, R. M., San Martini, F., Sheehy, P. M., Zahniser, M. S., Shorter, J. H., Wormhoudt, J. C., Lamb, B. K., Allwine, E. J., Gaffney, J. S., Marley, N. A., Grutter, M., Marquez, C., Blanco, S., Cardenas, B., Retama, A., Ramos Villegas, C. R., Kolb, C. E., Molina, L. T., and Molina, M. J. : Evaluation of nitrogen dioxide chemiluminescence monitors in a polluted urban environment, Atmos. Chem. Phys., 7, 2691-2704, 2007.

Folberth, G. A., Hauglustaine, D. A., Lathière, J., and Brocheton, F. : Interactive chemistry in the Laboratoire de Météorologie Dynamique general circulation model : model description and impact analysis of biogenic hydrocarbons on tropospheric chemistry, Atmos. Chem. Phys., 6, 2273–2319, 2006.

Franco, V., Kousoulidou, M., Muntean, M., Ntziachristos, L., Hausberger, S., and Dilara, P. : Road vehicle emission factors development : A review, Atmos. Environ., 70, 84–97, 2013.

Freney, E. J., Sellegri, K., Canonaco, F., Colomb, A., Borbon, A., Michoud, V., Doussin, J.-F., Crumeyrolle, S., Amarouch, N., Pichon, J.-M., Prévôt, A. S. H., Beekmann, M., and Schwarzenböeck, A. : Characterizing the impact of urban emissions on regional aerosol particles ; airborne measurements during the MEGAPOLI experiment, Atmos. Chem. Phys. Discus., 13, 24 885–24 924, 2013.

Gilliland, A. and Abbitt, P. J. : A sensitivity study of the discrete Kalman filter (DKF) to initial condition discrepancies, J. Geophys. Res., 106, 17 939, 2001.

Granier, C., Bessagnet, B., Bond, T., D'Angiola, A., Denier van der Gon, H. A. C., Frost, G. J., Heil, A., Kaiser, J. W., Kinne, S., Klimont, Z., Kloster, S., Lamarque, J.-F., Liousse, C., Masui, T., Meleux, F., Mieville, A., Ohara, T., Raut, J.-C., Riahi, K., Schultz, M. G., Smith, S. J., Thompson, A., Aardenne, J., Werf, G. R., and Vuuren, D. P. : Evolution of anthropogenic and biomass burning emissions of air pollutants at global and regional scales during the 1980-2010 period, Climatic Change, 109, 163–190, 2011.

Guenther, A., Karl, T., Harley, P., Wiedinmyer, C., Palmer, P. I., and Geron, C. : Estimates of global terrestrial isoprene emissions using MEGAN (Model of Emissions of Gases and Aerosols from Nature), Atmos. Chem. Phys., 6, 3181-3210, 2006.

Haeffelin, M., Angelini, F., Morille, Y., Martucci, G., Frey, S., Gobbi, G. P., Lolli, S., O'Dowd, C. D., Sauvage, L., Xueref-Rémy, I., Wastine, B., and Feist, D. G. : Evaluation of Mixing-Height Retrievals from Automatic Profiling Lidars and Ceilometers in View of Future Integrated Networks in Europe, Bound.-Lay. Meteorol., 143, 49–75, 2012.

Hakami, A., Henze, D. K., Seinfeld, J. H., Chai, T., Tang, Y., Carmichael, G. R., and Sandu, A. : Adjoint inverse modeling of black carbon during the Asian Pacific Regional Aerosol Characterization Experiment, J. Geophys. Res., 110, D14 301, 2005.

Hanna, S. R., Lu, Z., Christopher Frey, H., Wheeler, N., Vukovich, J., Arunachalam, S., Fernau, M., and Alan Hansen, D. : Uncertainties in predicted ozone concentrations due to input uncertainties for the UAM-V photochemical grid model applied to the July 1995 OTAG domain, Atmos. Environ., 35, 891–903, 2001.

Hansen, M. C. and Reed, B. : A comparison of the IGBP DISCover and University of Maryland 1 km global land cover products, Int. J. Remote Sens., 21, 1365–1373, 2000.

Hansen, M. C., Defries, R. S., Townshend, J. R. G., and Sohlberg, R. : Global land cover classification at 1 km spatial resolution using a classification tree approach, Int. J. Remote Sens., 21, 1331–1364, 2000.

Hauglustaine, D. A., Hourdin, F., Jourdain, L., Filiberti, M.-A., Walters, S., Lamarque, J.-F., and Holland, E. A. : Interactive chemistry in the Laboratoire de Meteorology Dyanmique general

circulation model: Description and background tropospheric chemistry evaluation, J. Geophys. Res., 109, D04314, 2004.

Healy, R. M., Sciare, J., Poulain, L., Kamili, K., Merkel, M., Müller, T., Wiedensohler, A., Eckhardt, S., Stohl, A., Sarda-Estève, R., McGillicuddy, E., O'Connor, I. P., Sodeau, J. R., and Wenger, J. C. : Sources and mixing state of size-resolved elemental carbon particles in a European megacity : Paris, Atmos. Chem. Phys., 12, 1681–1700, 2012.

Junker, C. and Liousse, C. : A global emission inventory of carbonaceous aerosol from historic records of fossil fuel and biofuel consumption for the period 1860-1997, Atmos. Chem. Phys., 8, 1195–1207, 2008.

Konovalov, I. B., Beekmann, M., Richter, A., and Burrows, J. P. : Inverse modelling of the spatial distribution of NO_x emissions on a continental scale using satellite data, Atmos. Chem. Phys., 6, 1747–1770, 2006.

Konovalov, I. B., Beekmann, M., Burrows, J. P., and Richter, A. : Satellite measurement based estimates of decadal changes in European nitrogen oxides emissions, Atmos. Chem. Phys., 8, 2623–2641, 2008.

Lamarque, J.-F., Bond, T. C., Eyring, V., Granier, C., Heil, A., Klimont, Z., Lee, D., Liousse, C., Mieville, A., Owen, B., Schultz, M. G., Shindell, D., Smith, S. J., Stehfest, E., Van Aardenne, J., Cooper, O. R., Kainuma, M., Mahowald, N., McConnell, J. R., Naik, V., Riahi, K., and van Vuuren, D. P. : Historical (1850-2000) gridded anthropogenic and biomass burning emissions of reactive gases and aerosols : methodology and application, Atmos. Chem. Phys., 10, 7017–7039, 2010.

Liousse, C., Cachier, H., and Jennings, S. G. : Optical and thermal measurements of black carbon aerosol content in different environments: variation of the specific attenuation cross-section, sigma (σ), Atmos. Env., 27A, 8, 1203-1211, 1993.

Lohmann, U. and Feichter, J. : Global indirect aerosol effects : a review, Atmos. Chem. Phys., 5, 715–737, 2005.

McNaughton, C. S., Clarke, A. D., Howell, S. G., Pinkerton, M., Anderson, B., Thornhill, L., Hudgins, C., Winstead, E., Dibb, J. E., Scheuer, E., and Maring, H. : Results from the DC-8 Inlet Characterization Experiment (DICE) : Airborne Versus Surface Sampling of Mineral Dust and Sea Salt Aerosols, Aerosol Sci. Tech., 41, 136–159, 2007.

Mendoza-Dominguez, A. and Russell, A. G. : Iterative Inverse Modeling and Direct Sensitivity Analysis of a Photochemical Air Quality Model, Environ. sci. technol., 34, 4974–4981, 2000.

Menut, L., Bessagnet, B., Khvorostyanov, D., Beekmann, M., Blond, N., Colette, A., Coll, I., Curci, G., Foret, G., Hodzic, A., Mailler, S., Meleux, F., Monge, J.-L., Pison, I., Siour, G., Turquety, S., Valari, M., Vautard, R., and Vivanco, M. G. : CHIMERE 2013 : a model for regional atmospheric composition modelling, Geoscientific Model Development, 6, 981–1028, 2013.

1 Napelenok, S. L., Pinder, R. W., Gilliland, A. B., and Martin, R. V. : A method for evaluating
2   spatially-resolved NO_x emissions using Kalman filter inversion, direct sensitivities, and space-
3   based NO_2 observations, Atmos. Chem. Phys. Discus., 8, 6469–6499, 2008.

4 Napelenok, S. L., Foley, K. M., Kang, D., Mathur, R., Pierce, T., and Rao, S. T. : Dynamic
5   evaluation of regional air quality model's response to emission reductions in the presence of
6   uncertain emission inventories, Atmos. Environ., 45, 4091–4098, 2011.

7 Nenes, A., Pandis, S., and Pilinis, C. : ISORROPIA : A New Thermodynamic Equilibrium Model for
8   Multiphase Multicomponent Inorganic Aerosols, Aquat. geochem., pp. 123–152, 1998.

9 Parrish, D. D. : Critical evaluation of US on-road vehicle emission inventories, Atmos. Environ., 40,
10   2288–2300, 2006.

11 Peng, R. D., Bell, M. L., Geyh, A. S., McDermott, A., Zeger, S. L., Samet, J. M., and Dominici, F. :
12   Emergency admissions for cardiovascular and respiratory diseases and the chemical
13   composition of fine particle air pollution., Environ. Health Persp., 117, 957–63, 2009.

14 Petetin, H., Beekmann, M., Sciare, J., Bressi, M., Rosso, A., Sanchez, O., and Ghersi, V. : A novel
15   model evaluation approach focussing on local and advected contributions to urban PM2.5
16   levels - application to Paris, France, Geoscientific Model Development Discussions, 6, 6391–
17   6457, 2013.

18 Petzold, A., Ogren, J. A., Fiebig, M., Laj, P., Li, S.-M., Baltensperger, U., Holzer-Popp, T., Kinne,
19   S., Pappalardo, G., Sugimoto, N., Wehrli, C., Wiedensohler, A., and Zhang, X.-Y. :
20   Recommendations for the interpretation of "black carbon" measurements, Atmos. Chem. Phys.
21   Discus., 13, 9485–9517, 2013.

22 Pouliot, G., Pierce, T.E., Denier van der Gon, H., Schaap, M., Moran, M., Nopmongeol, U. :
23   Comparing emission inventories and model-ready emission datasets between Europe and North
24   America for the AQMEII project. Atmos. Environ. 53, 4–14, 2012.

25 Schmidt, H., Derognat, C., Vautard, R., and Beekmann, M. : A comparison of simulated and
26   observed ozone mixing ratios for the summer of 1998 in Western Europe, Atmos. Environ., 35,
27   6277–6297, 2001.

28 Schulz, M., Textor, C., Kinne, S., Balkanski, Y., Bauer, S., Berntsen, T., Berglen, T., Boucher, O.,
29   Dentener, F., Guibert, S., Isaksen, I. S. A., Iversen, T., Koch, D., Kirkevåg, A., Liu, X.,
30   Montanaro, V., Myhre, G., Penner, J. E., Pitari, G., Reddy, S., Seland, O., Stier, P., and
31   Takemura, T. : Radiative forcing by aerosols as derived from the AeroCom present-day and
32   pre-industrial simulations, Atmos. Chem. Phys., 6, 5225-5246, 2006.

33 Sciare, J., d'Argouges, O., Sarda-Estève, R., Gaimoz, C., Dolgorouky, C., Bonnaire, N., Favez, O.,
34   Bonsang, B., and Gros, V. : Large contribution of water-insoluble secondary organic aerosols
35   in the region of Paris (France) during wintertime, J. Geophys. Res., 116, D22203, 2011.

Skamarock, W. C., Klemp, J. B., Gill, D. O., Barker, D. M., and Powers, J. G. : A Description of the Advanced Research WRF Version 2, Tech. Rep., 2005.

Smit, R., Ntziachristos, L., and Boulter, P. : Validation of road vehicle and traffic emission models - A review and meta-analysis, Atmos. Environ., 44, 2943–2953, 2010.

Tian, D., Cohan, D. S., Napelenok, S., Bergin, M., Hu, Y., Chang, M., and Russell, A. G. : Uncertainty Analysis of Ozone Formation and Response to Emission Controls Using Higher-Order Sensitivities, J. Air Waste Manage., 60, 797–804, 2010.

Timmermans, R., Denier van der Gon, H.A.C., Kuenen, J.J.P., Segers, A.J., Honoré, C., Perrussel, O., Builtjes, P.J.H., and Schaap, M. : Quantification of the urban air pollution increment and its dependency on the use of down-scaled and bottom- up city emission inventories, Urban Climate 6 (2013) 44–62, 2013

Troen, I. B. and Mahrt, L. : A simple model of the atmospheric boundary layer ; sensitivity to surface evaporation, Bound.-Lay. Meteorol., 37, 129–148, 1986.

Vautard, R., Martin, D., Beekmann, M., Drobinski, P., Friedrich, R., Jaubertie, A., Kley, D., Lattuati, M., Moral, P., Neininger, B., Theloke, J.: Paris emission inventory diagnostics from ESQUIF airborne measurements and a chemistry transport model, J. Geophys. Res., 108, 8564, 2003.

Vestreng, V., Mareckova, K., Kakareka, S., Malchykhina, A., and Kukharchyk, T. : Inventory Review 2007 - Emission data reported to LRTAP Convention and NEC Directive, Tech. rep., 2007.

Vignati, E., Karl, M., Krol, M., Wilson, J., Stier, P., and Cavalli, F. : Sources of uncertainties in modelling black carbon at the global scale, Atmos. Chem. Phys., 10, 2595–2611, 2010.

Virkkula, A., Ahlquist, N. C., Covert, D. S., Arnott, W. P., Sheridan, P. J., Quinn, P. K., and Coffman, D. J. : Modification, Calibration and a Field Test of an Instrument for Measuring Light Absorption by Particles, Aerosol Sci. Tech., 39, 68–83, 2005.

Xu, W., Zhao, C., Ran, L., Deng, Z., Ma, N., Liu, P., Lin, W., Yan, P., and Xu, X. : A new approach to estimate pollutant emissions based on tra jectory modeling and its application in the North China Plain, Atmos. Environ., 71, 75–83, 2013.

Yu, H., Kaufman, Y. J., Chin, M., Feingold, G., Remer, L. A., Anderson, T. L., Balkanski, Y., Bellouin, N., Boucher, O., Christopher, S., DeCola, P., Kahn, R., Koch, D., Loeb, N., Reddy, M. S., Schulz, M., Takemura, T., and Zhou, M. : A review of measurement-based assessments of the aerosol direct radiative effect and forcing, Atmos. Chem. Phys., 6, 613–666, 2006.

Zhang, Q. J., Beekmann, M., Drewnick, F., Freutel, F., Schneider, J., Crippa, M., Prevot, A. S. H., Baltensperger, U., Poulain, L., Wiedensohler, A., Sciare, J., Gros, V., Borbon, A., Colomb, A., Michoud, V., Doussin, J.-F., Denier van der Gon, H. A. C., Haeffelin, M., Dupont, J.-C., Siour, G., Petetin, H., Bessagnet, B., Pandis, S. N., Hodzic, A., Sanchez, O., Honoré, C., and Perrussel, O.: Formation of organic aerosol in the Paris region during the MEGAPOLI summer

campaign: evaluation of the volatility-basis-set approach within the CHIMERE model, Atmos. Chem. Phys., 13, 5767-5790, doi:10.5194/acp-13-5767-2013, 2013.

Zhou, X., Gao, J., Wang, T., Wu, W., and Wang, W. : Measurement of black carbon aerosols near two Chinese megacities and the implications for improving emission inventories, Atmos. Environ., 43, 3918–3924, 2009.